JBC RESEARCH ARTICLE

TFPI2 suppresses the interaction of TGF-β2 pathway regulators to promote endothelial–mesenchymal transition in diabetic nephropathy

Received for publication, August 10, 2021, and in revised form, January 25, 2022 Published, Papers in Press, February 11, 2022,
https://doi.org/10.1016/j.jbc.2022.101725

Guoying Guan[1], **Jinjiao Xie**[1], **Yamei Dai**[2], **and Hui Han**[1,*]

From the [1]*Department of Geriatrics and* [2]*Health Management Center, The First Affiliated Hospital of Harbin Medical University, Harbin, Heilongjiang, People's Republic of China*

Edited by Qi Qun Tang

Endothelial–mesenchymal transition (EndMT) is an important source of myofibroblasts, but also contributes to the progression of diabetic nephropathy (DN). By several differential gene expression analyses from the Gene Expression Omnibus (GEO) database, the tissue factor pathway inhibitor 2 (*TFPI2*) gene, known as a tumor suppressor, was shown to be dysregulated in DN; however, the potential role and regulatory mechanism of TFPI2 in DN are unclear. Here, we found abnormal upregulation of TFPI2 in the renal cortex of diabetic mice, accompanied by impaired renal function. We also injected a single dose of adeno-associated virus (AAV)2 carrying shRNA targeting *TFPI2* intravenously into these mice and found that knockdown of *TFPI2* improved renal function and reduced renal fibrosis and cell apoptosis in experimental DN. Furthermore, hyperglycemia-induced EndMT was inhibited in the absence of *TFPI2*, as evidenced by increased expression of endothelial markers (VE-cadherin and CD31) and decreased expression of mesenchymal markers (α-SMA, desmin, and FSP-1). To further explore the mechanism *in vitro*, human renal glomerular endothelial cells (hRGECs) were incubated in the presence of high glucose or transforming growth factor beta (TGF-β)2. *TFPI2* deficiency inhibited high glucose-induced cell apoptosis and TGF-β2-induced EndMT in hRGECs, while overexpression of TFPI2 had the opposite effects. Importantly, TGF-β2 is a crucial driver of EndMT, and we found that TFPI2 promoted TGF-β2/Smad signaling activation by interferring the interaction of TGF-β pathway regulators (SMURF2 with SMAD7). Our results show that TFPI2 regulates EndMT and the TGF-β2 signaling pathway and is a potential promoter of DN pathogenesis.

Diabetic nephropathy (DN) is a leading cause of end-stage renal disease globally. Approximately 40% of DN patients are accompanied with diabetes mellitus (1). With increasing prevalence of diabetes, there is a parallel worldwide rise in the incidence of DN (2, 3). Increasing mortality in patients with diabetes is predominately attributed to kidney disease (4). The symptoms of DN generally do not develop until kidney function has been severely impaired. Management of diabetes is essential for therapies against DN, and a long-term tight glycemic control is well established for prevention of DN in early course of diabetes (5, 6). However, there is still a large risk of DN progression in long-standing diabetes or after onset of complications (7). To cure or prevent DN, a better understanding of the pathogenesis of DN and developing novel strategies that not directly act on normalizing blood glucose are required.

Renal fibrosis is the final pathological events of DN, leading to destruction of kidney structure and loss of kidney function (8, 9). Fibrosis in the kidney results from prolonged injury accompanied with aberrant wound healing process and excessive accumulation of extracellular matrix (ECM). Renal myofibroblasts are essential mediators in fibrotic process (10). There are diverse origins of myofibroblasts that are responsible for producing ECM, depending on the organ and injury type. In general, resident renal fibroblasts, epithelial–mesenchymal transition (EMT), pericytes, mesangial cells, and bone marrow–derived cells are the main sources of myofibroblasts in the kidney (11). Particularly, endothelial–mesenchymal transition (EndMT), a process involving in endothelial cells, is recently considered as an important source of myofibroblasts in diabetic renal fibrosis (12, 13). Endothelial cells that undergo EndMT process acquire myofibroblast features with ability to present fibrogenesis-related mesenchymal cell characteristics and involve in renal fibrosis (14, 15). Studies have shown that inhibiting the occurrence of EndMT can reduce kidney fibrosis and improve kidney function (16, 17). Therefore, EndMT is a promising therapeutic target for DN treatment.

Transforming growth factor beta (TGF-β) is a primary driver of EndMT, and it induces kidney fibrosis largely *via* activating its downstream Smad-dependent and independent signaling (18). TGF-β/Smad singling is closely linked with the pathogenesis of DN. Upregulation of TGF-β isoforms and their receptors has been found in the kidney of human and experimental DN (19, 20). TGF-β initiates the intracellular signaling by binding to TGF-β receptors (TGFBRs), resulting in phosphorylation of specific Smad proteins, SMAD2 and SMAD3. Upon activation, these Smad proteins translocate into

* For correspondence: Hui Han, hydyyqkgp@163.com.

the nucleus and thus regulate the transcriptional expression of target genes (21). The importance of TGF-β/Smad signaling in fibrosis in DN suggests it as a potent therapeutic target for DN.

Tissue factor pathway inhibitor 2 (TFPI2) belongs to Kunitz-type serine proteinase inhibitor family. It is predominately synthesized by endothelial cells derived from different blood vessels (22). TFPI2 is expressed in various human tissues, such as the kidney, liver, heart, pancreas, breast, and skeletal muscle (23, 24). TFPI2 is increasingly considered as a tumor suppressor gene and has been found to induce caspase-mediated cell apoptosis in multiple tumors (25, 26). Recently, Ivanciu *et al.* showed that overexpression of TFPI2 inhibited endothelial cell angiogenesis and increased cell apoptosis (27). Having observed its proapoptotic potential, Ma and coworkers identified that recombinant TFPI2 attenuated proliferative glomerulonephritis and improved renal function by increasing mesangial cell apoptosis (28, 29). On the other hand, the apoptosis-promoting effect of TFPI2 on normal kidney cells could deteriorate renal function. These findings suggest that TFPI2 may function differently under different pathological conditions, which accounts for its potential beneficial and deleterious aspects. The role and regulatory mechanism of TFPI2 in other kidney disease, including DN, deserve more exploration.

In this study, we investigated TFPI2's role in DN through loss- and gain-of function experiments *in vivo* and *in vitro*. Its regulation on TGF-β/Smad signaling and the molecular mechanism were explored as well. Our study may provide novel insights into the pathogenesis of DN and suggest a potential therapeutic approach to DN.

Results

Increased expression of TFPI2 in mouse models of type 2 diabetes mellitus (T2DM)

Several differential gene expression analyses from Gene Expression Omnibus (GEO) database showed that TFPI2 is highly expressed in both glomeruli and tubules of DN patients (GSE30528 and GSE30529), renal expression of TFPI2 was increased in DN patients (GSE1009), and TGF-β induced TFPI expression in HK-2 human renal tubular epithelial cells (GSE23338). Venn diagram displayed the overlap (TFPI2) of differential upregulation of genes from these data (Fig. 1*A*). Two mouse models of T2DM, streptozotocin (STZ)-induced diabetic C57BL/6 mice and genetically diabetic db/db mice, were used to study DN *in vivo*. The course of modeling was displayed as Figure 1*B*. The body weight was measured weekly during the modeling. Compared with the control mice, the level of blood glucose (Fig. 1*C*), serum levels of blood urea nitrogen (BUN) (Fig. 1*D*), creatinine (Fig. 1*E*), neutrophil gelatinase-associated lipocalin (NGAL) (Fig. 1*F*) and periostin (Fig. 1*G*), and content of 24-h urine protein (Fig. 1*H*) were significantly higher in both STZ-induced diabetic mice and db/db mice. Immunofluorescent staining (Fig. 2, *A* and *D*), real-time PCR (Fig. 2, *B* and *E*), and Western blot analysis (Fig. 2, *C* and *F*) showed that the expression of TFPI2 was markedly higher in renal cortex of diabetic mice than that in controls. Loss of positive immunostaining of CD31, an endothelial marker, might indicate endothelial cell loss or transformation in renal cortex of STZ-induced diabetic mice and db/db mice (Fig. 2, *A* and *D*). These findings suggest that dysregulation of TFPI2 may be related to the pathogenesis of DN.

Knockdown of TFPI2 improves kidney function

To investigate the role of TFPI2 in DN, loss-of-function experiment for TFPI2 was carried out *in vivo*. STZ-treated mice were intravenously injected with adeno-associated virus (AAV)2 carrying shRNA targeting TFPI2 (TFPI2 shRNA) or negative control (NC) shRNA. The expression of TFPI2 was efficiently downregulated in renal cortex at both mRNA and protein levels (Fig. 3, *A* and *B*). Inhibition of TFPI2 reduced STZ-induced serum levels of BUN (Fig. 3*C*), creatinine (Fig. 3*D*), NGAL (Fig. 3*E*) and periostin (Figs. 3*F*), and 24-h urine protein content (Fig. 3*G*). Similarly, db/db mice displayed these alterations in renal cortex after knockdown of TFPI2 (Fig. 3, *H*–*N*). Moreover, histological analysis of consecutive renal sections revealed that upregulation of TFPI2 was accompanied with increased periodate Schiff (PAS) glycogen staining in diabetic mice (Fig. 3, *O* and *P*). In comparison, knockdown of TFPI2 decreased glycogen in renal cortex.

Knockdown of TFPI2 inhibits cell apoptosis in kidney

Cell apoptosis in renal cortex was evaluated by TUNEL staining (Fig. 4, *A* and *D*). Downregulation of TFPI2 attenuated cell apoptosis in STZ-induced diabetic mice (Fig. 4*A*) and db/db mice (Fig. 4*D*). The expression of apoptosis-related proteins including pro- and cleaved caspase 3 and pro- and cleaved caspase 7 was detected in renal cortex by Western blot (Fig. 4, *B* and *E*). Quantitative analysis showed a significant reduction in the relative expression ratio of cleaved to pro-caspase 3/7 following TFPI2 knockdown (Fig. 4, *C* and *F*).

Knockdown of TFPI2 attenuates renal fibrosis and EndMT

Masson staining was carried out to examine renal fibrosis. To investigate the effect of TFPI2 on renal fibrosis, we firstly performed immunostaining for TFPI2 and Masson staining using consecutive sections of renal cortex (Fig. 5, *A* and *B*). Diabetic mice displayed server fibrosis in renal cortex with higher expression of TFPI2, and the areas with low expression of TFPI2 showed less masson staining. The results suggested the potential contribution of TFPI2 to renal fibrosis. Further, Western blot analysis showed that the expression of α-SMA, desmin, and fibroblast-specific protein 1 (FSP-1) was upregulated, and VE-cadherin was downregulated in renal cortex of STZ-treated mice (Fig. 5, *C*–*G*) and db/db mice (Fig. 5, *H*–*L*). Knockdown of TFPI2 reversed the expression alterations in these proteins, indicating that TFPI2 might promote EndMT and its inhibition might suppress the process.

TFPI2 enhances high glucose-induced cell apoptosis

We further investigate the function of TFPI2 *in vitro* under a high-glucose atmosphere. Human renal glomerular

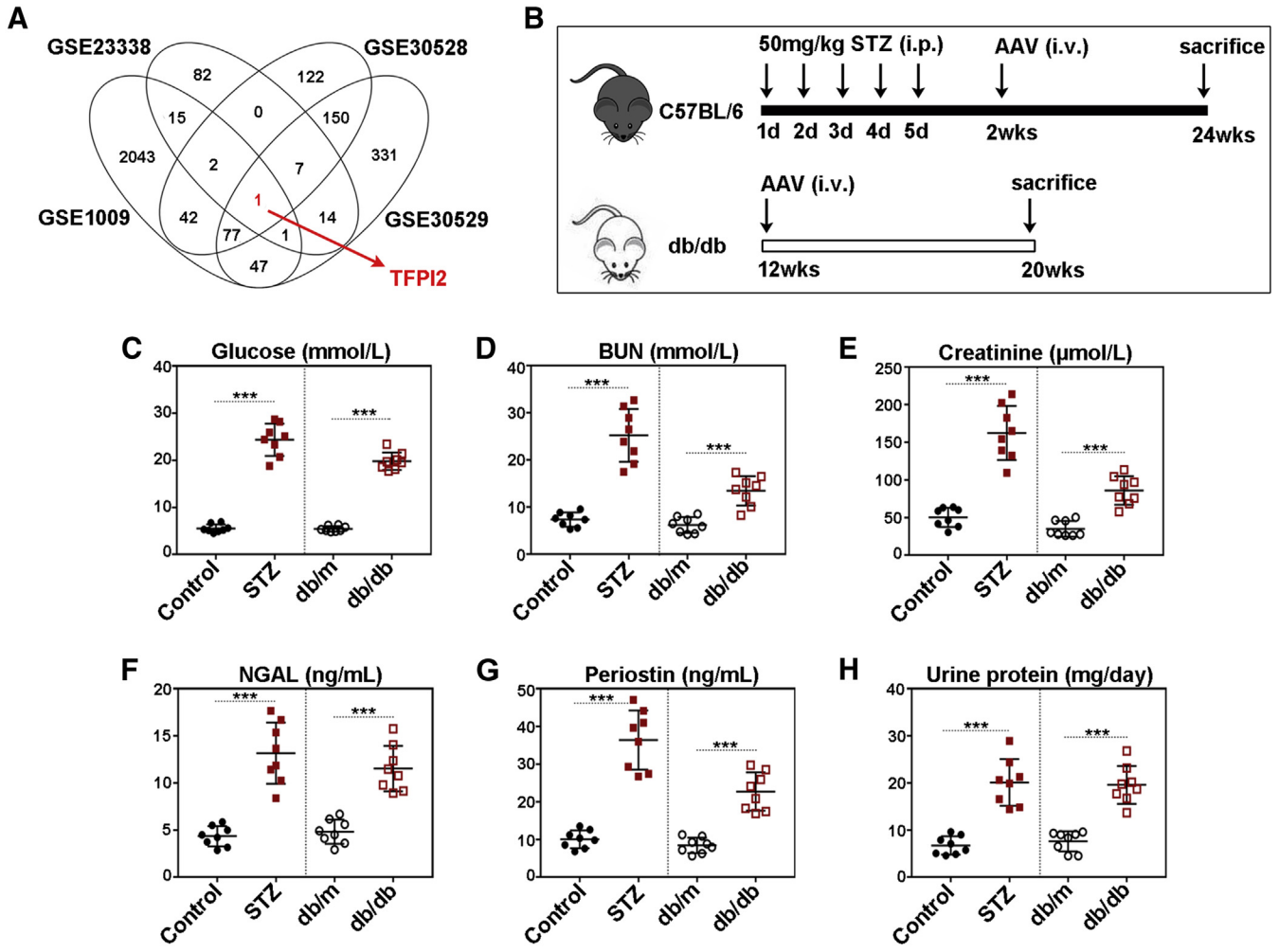

Figure 1. Establishment of experimental DN in mice. *A,* Venn diagram showing the overlap (TFPI2) of several differential gene expression analyses in diabetic nephropathy from Gene Expression Omnibus (GEO) database (GSE23338, GSE30528, GSE1009, and GSE30529). *B,* schematic diagram of T2DM mouse modeling. STZ-induced diabetic C57BL/6 mice and genetically diabetic db/db mice were used to study DN *in vivo*. *C,* the levels of blood glucose were detected following gavage administration of 2 g/kg glucose solution at the end of modeling. The serum levels of (*D*) blood urea nitrogen (BUN), (*E*) creatinine, (*F*) neutrophil gelatinase-associated lipocalin (NGAL), and (*G*) periostin in STZ-induced mice and db/db mice. *H,* examination of 24-h urine protein level. Data are shown as the mean ± SD (n = 8). ***$p < 0.001$. DN, diabetic nephropathy; T2DM, type 2 diabetes mellitus.

endothelial cells (hRGECs) were identified by CD31-positive immunostaining (Fig. 6*A*). Flow cytometric analysis showed that cell apoptosis was significantly increased after treatment with 30 mM glucose for 48 h (Fig. 6*B*). Consistently, the relative expression ratio of cleaved to pro-caspase 3/7 was elevated in high glucose-treated hRGECs (Fig. 6, *C*, *E*, and *F*). Cells were infected with adenovirus carrying TFPI2 shRNA or expressing TFPI2 (TFPI2 OE), followed by treatment with 30 mM glucose. The infection efficiency was verified by Western blot (Fig. 6, *C* and *D*). High-glucose-induced cell apoptosis and apoptotic protein expression were abolished by inhibition of TFPI2, while aggravated by overexpression of TFPI2 (Fig. 6, *B*–*F*).

TGF-β2 stimulation induces the expression of TFPI2 in vitro

TGF-β is crucial for inducing EndMT and fibrosis, and TGF-β2 was used as an inducer of EndMT in hRGECs in the present study. To study the expression of TFPI2 and SMURF2 under TGF-β2 stimulation, hRGECs were treated with 0, 1, 2.5, 5, or 10 ng/ml of TGF-β2 for 0, 12, 24, or 48 h. The expression of TFPI2 was increased along with TGF-β2 concentration and incubation time (Fig. 7, *A* and *B*). It seemed that SMURF2 expression reached the highest under 5 ng/ml of TGF-β2 stimulation. We further explore the potential mechanism of TGF-β2-induced TFPI2 expression. According to JASPAR database, TFPI2 is predicted as a potential target gene of SMAD2/3/4. We hypothesized that TGF-β/Smad signal might promote TFPI2 transcription and thus increase its expression. Dual-luciferase reporter assay was performed to assess the promoter activity of TFPI2 gene under TGF-β2 stimulation. The results showed that stimulation with higher concentration of TGF-β2 resulted in higher luciferase activity, indicating that TGF-β2 stimulation might regulate TFPI2 promoter activity (Fig. 7*C*). Further, the expression of TFPI2 was decreased after knockdown of SMAD4 under 5 ng/ml TGF-β2 for 48 h (Fig. 7, *D* and *E*). Collectively, these data preliminarily verified that TFPI2 might be a direct target gene for TGF-β/Smad signal.

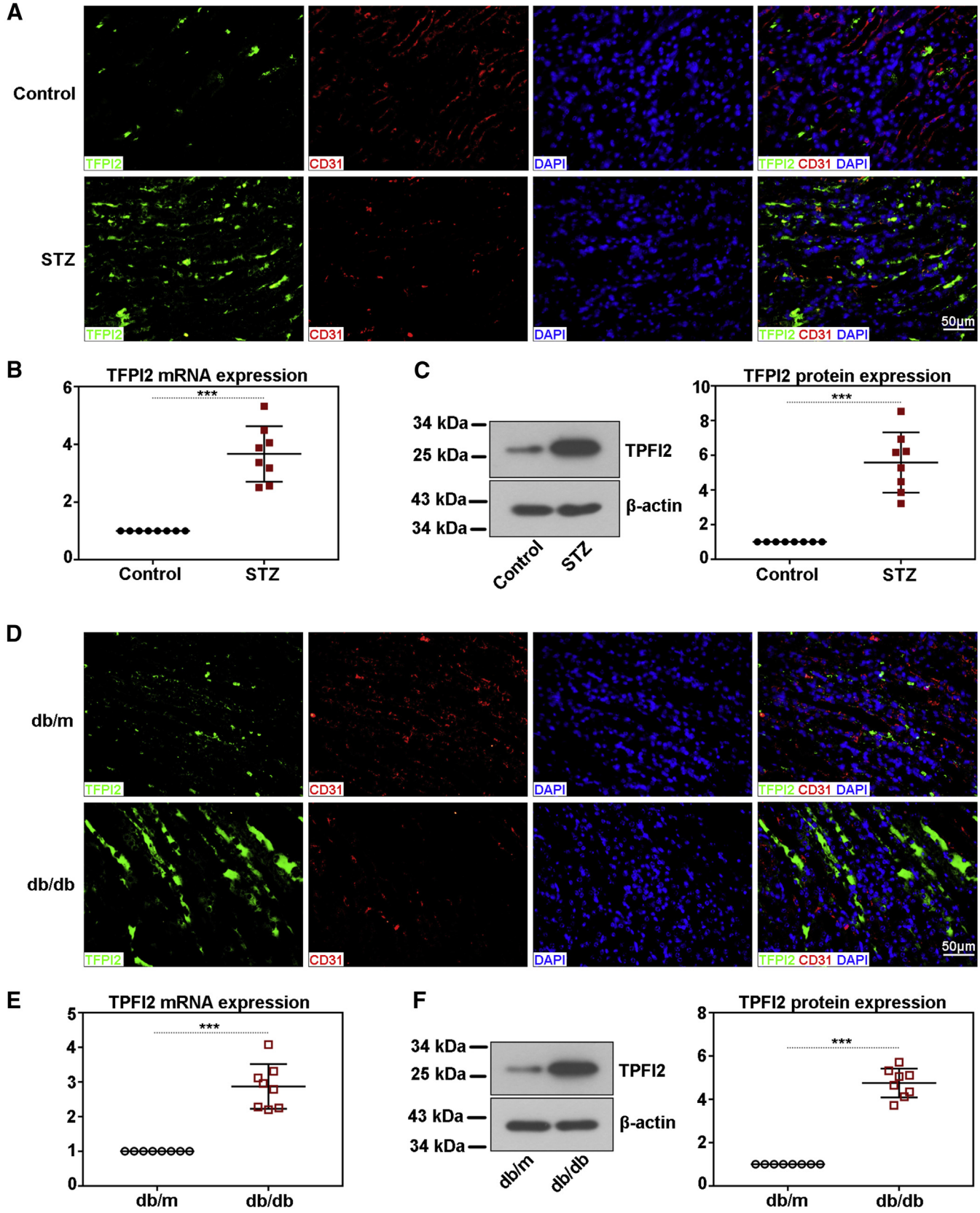

Figure 2. Expression of TFPI2 in STZ-induced diabetic mice and db/db mice. Two mouse models of T2DM including STZ-induced C57BL/6 mice and db/db mice were used to study DN *in vivo*. The expression of TFPI2 was examined in renal cortex tissues of diabetic mice. *A,* immunofluorescence for TFPI2 and CD31 in renal cortex tissues of STZ-treated mice. *B,* real-time PCR and (*C*) Western blotting analysis of TFPI2 mRNA and protein expression levels in renal cortex tissues of STZ-treated mice. *D,* immunofluorescence, (*E*) Real-time PCR, and (*F*) Western blot analysis for renal expression of TFPI2 in db/db mice. Data are shown as the mean ± SD (n = 8). ***$p < 0.001$. DN, diabetic nephropathy; STZ, streptozotocin; TFP12, tissue factor pathway inhibitor 2.

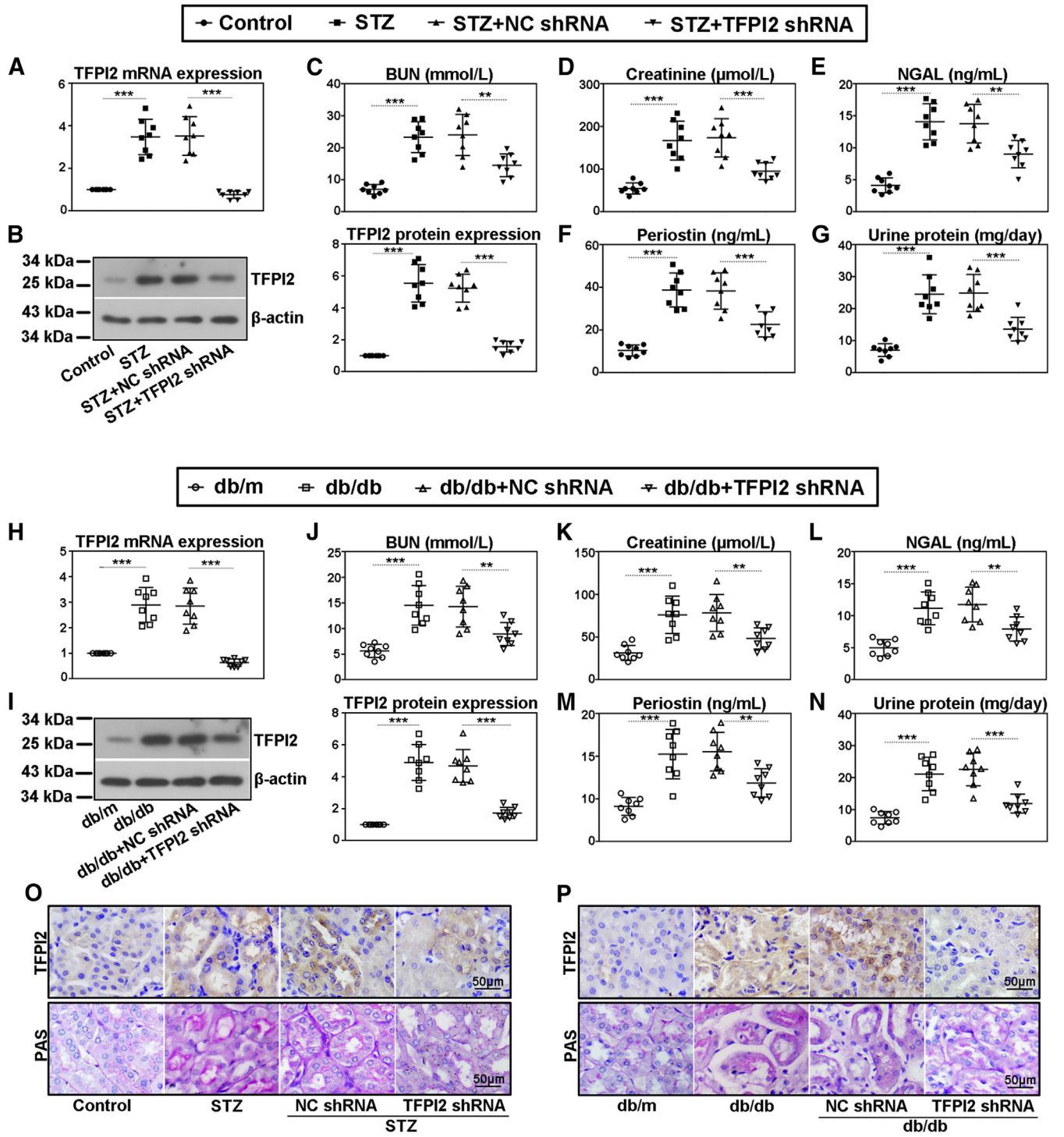

Figure 3. Knockdown of TFPI2 improves kidney function. Mice were intravenously injected with adeno-associated virus (AAV)2 carrying short hairpin RNA (shRNA) against TFPI2 to induce TFPI2-knockout mice. *A* and *B*, the efficiency of AAV2-mediated TFPI2 knockdown was examined in renal cortex tissues of STZ-induced diabetic mice by (*A*) real-time PCR and (*B*) Western blot. The serum levels of (*C*) BUN, (*D*) creatinine, (*E*) NGAL, and (*F*) periostin, and (*G*) 24-h urine protein content were examined in STZ-induced diabetic mice. *H* and *I*, renal expression of TFPI2 in db/db mice by (*H*) real-time PCR and (*I*) Western blot. The serum levels of (*J*) BUN, (*K*) creatinine, (*L*) NGAL, and (*M*) periostin, and (*N*) 24-h urine protein content were examined in db/db mice. *O* and *P*, histological analysis with immunostaining for TFPI2 and PAS staining for glycogen deposition in renal cortex using consecutive sections. Data are shown as the mean ± SD (n = 8). $^{**}p < 0.01$, $^{***}p < 0.001$. AAV, adeno-associated virus; BUN, blood urea nitrogen; NGAL, neutrophil gelatinase-associated lipocalin; TFP12, tissue factor pathway inhibitor 2.

TFPI2 promotes TGF-β2-induced EndMT in vitro

Having observed the involvement of TFPI2 in EndMT in renal cortex of diabetic mice, we would further confirm the regulation of TFPI2 on EndMT in hRGECs. TGF-β2-induced TFPI2 was efficiently downregulated after infection of adenovirus expressing TFPI2 shRNA and was upregulated after

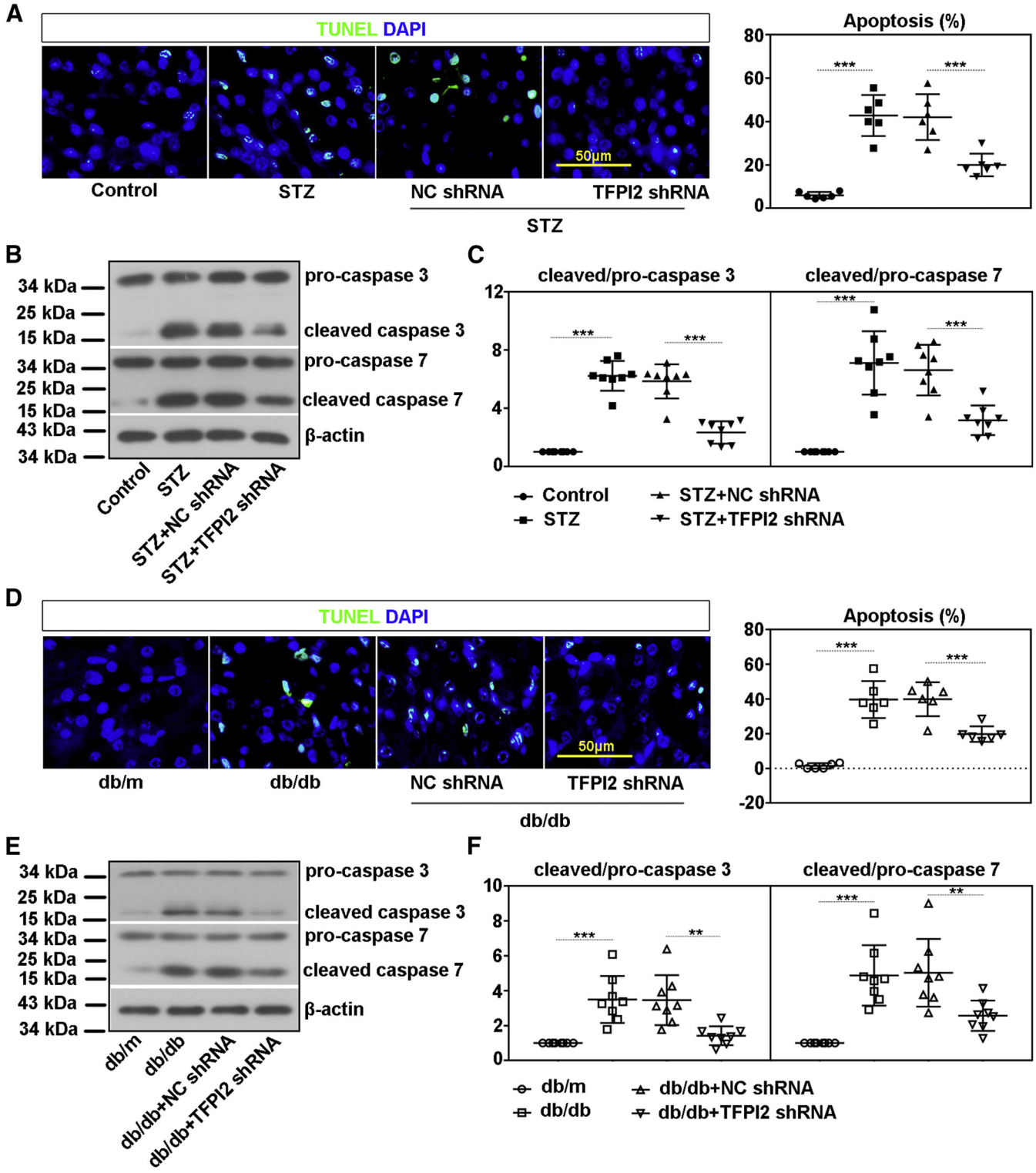

Figure 4. Knockdown of TFPI2 inhibits cell apoptosis in renal cortex. Cell apoptosis and several apoptotic proteins were examined in renal cortex of mice. *A*, TUNEL staining and quantitative analysis of cell apoptosis in renal cortex of STZ-treated mice. *B*, Western blotting for pro-caspase 3, cleaved caspase 3, pro-caspase 7 and cleaved caspase 7 in renal cortex tissues of STZ-treated mice. *C*, the ratio of the relative expression of cleaved caspase 3/7 to pro-caspase 3/7 (cleaved/pro-caspase 3/7). *D*, TUNEL staining of renal cortex in db/db mice. *E* and *F*, Western blotting for pro-caspase 3, cleaved caspase 3, pro-caspase 7 and cleaved caspase 7, and calculation of cleaved/pro-caspase 3/7 in renal cortex tissues of db/db mice. Data are shown as the mean ± SD (n = 8). $^{**}p < 0.01$, $^{***}p < 0.001$. EndMT, endothelial–mesenchymal transition; TFP12, tissue factor pathway inhibitor 2.

infection of adenovirus expressing TFPI2 OE (Fig. 8*A*). Immunofluorescent staining (Fig. 8*B*) together with Western blot analysis (Fig. 8, *C*–*G*) showed that TGF-β2 induced EndMT in hRGECs as evidenced by increased expression of mesenchymal markers α-SMA, desmin, and FSP-1 and decreased expression of VE-cadherin. Notably, TGF-β2-mediated EndMT was

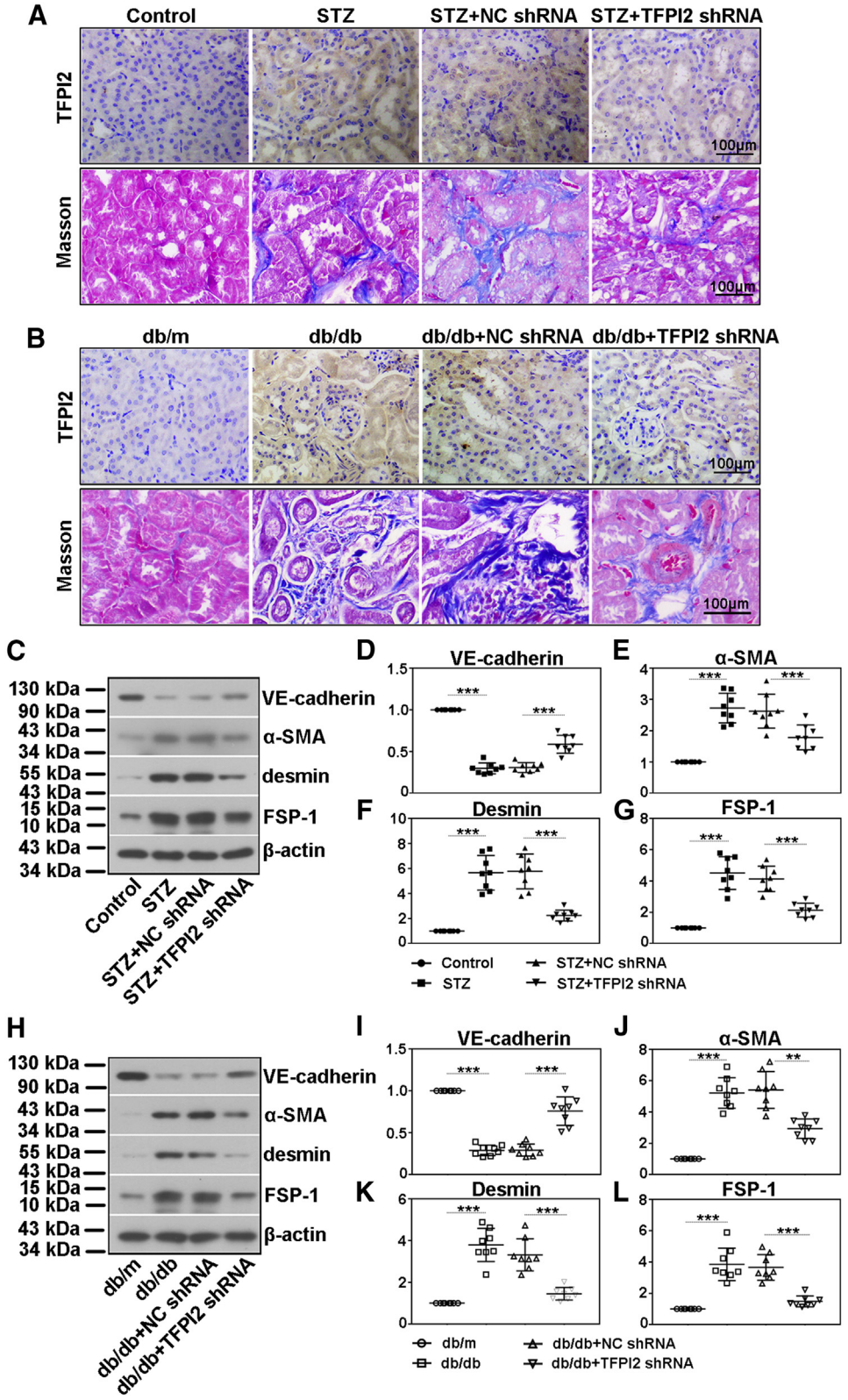

Figure 5. Knockdown of TFPI2 attenuates renal fibrosis and EndMT. *A* and *B*, immunostaining for TFPI2 and Masson staining for fibrosis in renal cortex using consecutive tissues. *C* and *H*, the expression of VE-cadherin, α-SMA, desmin, and FSP-1 in renal cortex was detected by Western blot. Semiquantitative analysis of (*D* and *I*) VE-cadherin, (*E* and *J*) α-SMA, (*F* and *K*) desmin, and (*G* and *L*) FSP-1. Data are shown as the mean ± SD (n = 8). $^{**}p < 0.01$, $^{***}p < 0.001$. EndMT, endothelial–mesenchymal transition; TFP12, tissue factor pathway inhibitor 2.

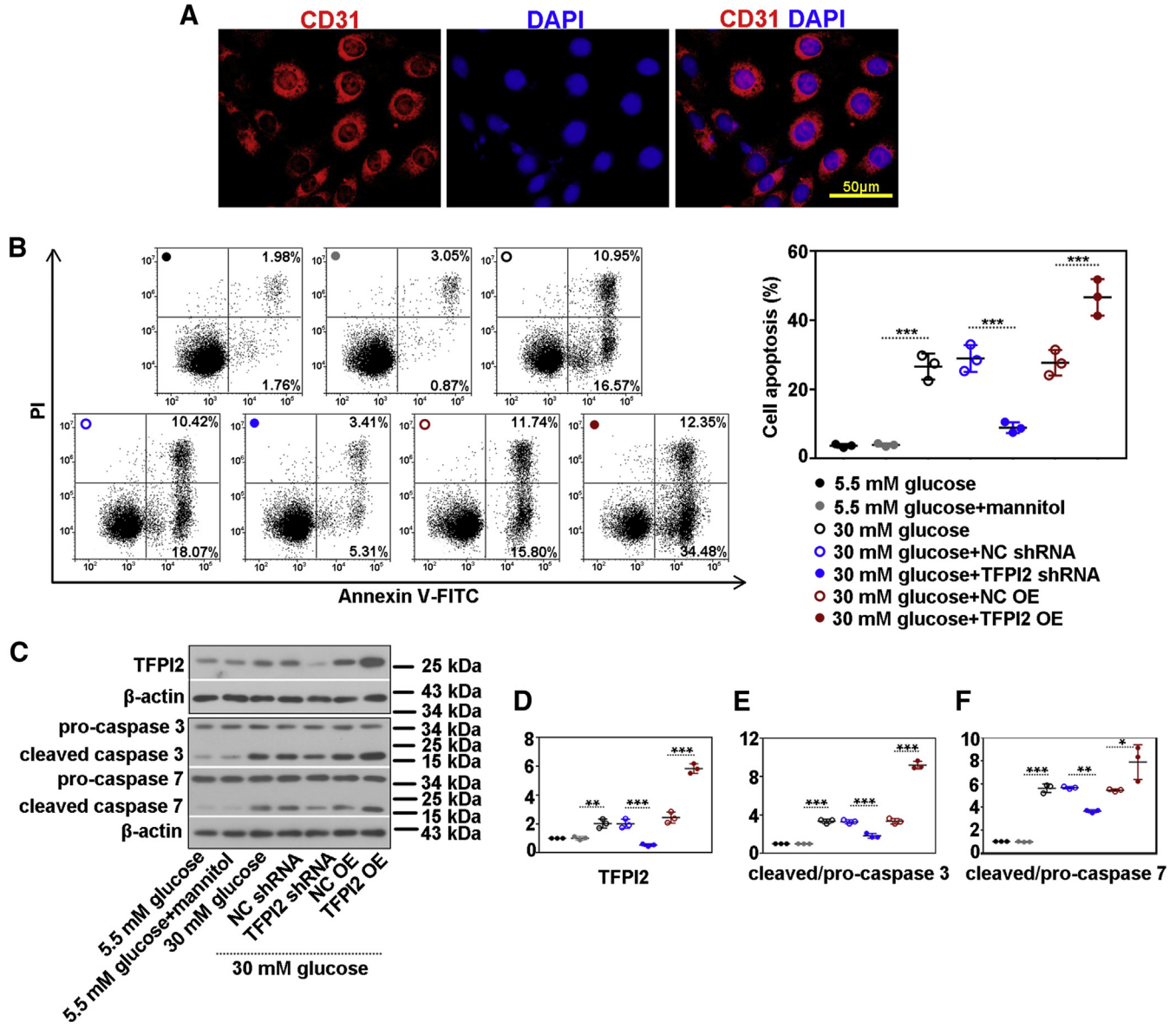

Figure 6. TFPI2 increases high-glucose-induced cell apoptosis. To study the effect of TFPI2 on cell apoptosis *in vitro,* human renal glomerular endothelial cells (hRGECs) were infected with adenovirus carrying TFPI2 shRNA (TFPI2 shRNA) or adenovirus expressing TFPI2 (TFPI2 OE). Twenty-four hours after infection, cells were treated with 30 mM glucose for 48 h. *A,* hRGECs was identified by positive immunolabeling of CD31. *B,* cell apoptosis was detected by flow cytometry with PI/Annexin V-FITC detection kit. *C,* the expression of TFPI2 and several apoptotic proteins (pro-caspase 3, cleaved caspase 3, pro-caspase 7 and cleaved caspase 7) was measured by Western blot. *D,* semiquantitative analysis of TFPI2. *E* and *F,* calculation of the ratio of the relative expression of cleaved caspase 3/7 to pro-caspase 3/7. Data are shown as the mean ± SD (n = 3). *$p < 0.05$, **$p < 0.01$, ***$p < 0.001$. hRGEC, human renal glomerular endothelial cell; TFP12, tissue factor pathway inhibitor 2.

suppressed by inhibition of TFPI2 and promoted by overexpression of TFPI2. These findings evidenced the contribution of TFPI2 to EndMT process *in vivo* and *in vitro*.

TFPI2 inhibits the interaction of SMURF2 with SMAD7 and regulates TGF-β/Smad signaling

It is known that TGF-β/Smad signaling pathway plays an important role in inducing EndMT and thus fibrosis (30). A previous study has proved that SMURF2 interacts with SMAD7 and then induces TGFBRs degradation, leading to inhibition of TGF-β signaling and TGF-β-induced EMT (31, 32). Based on a prediction of the interaction of TFPI2 and SMURF2, we here investigated whether TFPI2 influences SMURF2/SMAD7 complex formation and regulates TGF-β signaling. Firstly, the expression TFPI2 was observed to be negatively correlated with that of SMAD7 (Fig. 9, *A* and *B*), while positively correlated with TGFBR1 and TGFBR2 (Fig. 9, *A*, *C*, and *D*). The relative expression ratio of phosphor (p)-SMAD2/3 to SMAD2/3 was reduced by knockdown of TFPI2 and enhanced by overexpression of TFPI2 (Fig. 9, *A*, *E*, and *F*). In consistent with Western blot analysis, immunofluorescent staining confirmed that TFPI2 enhanced nuclear translocation of SMAD2 and SMAD3 in hRGECs under TGF-β2 stimulation (Fig. 9, *G* and *H*). Thus, TFPI2 could mediate SMAD2/3 activation.

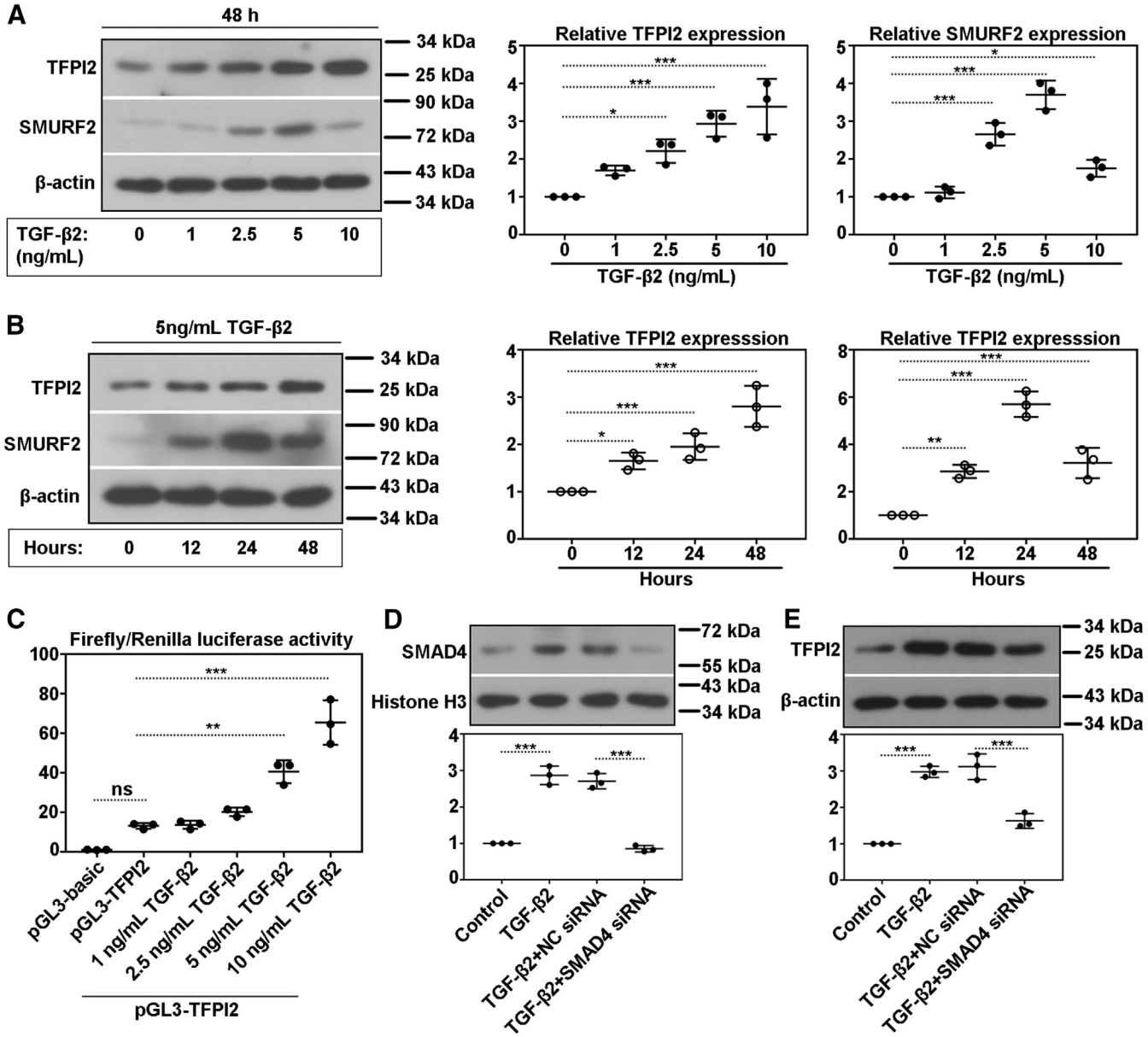

Figure 7. TGF-β2 induces expression of TFPI2 *in vitro*. Human renal glomerular endothelial cells (hRGECs) were incubated with human recombinant protein TGF-β2 to induce EndMT *in vitro*. *A,* the expression of TFPI2 and SMURF2 in hRGECs following treatment of 0, 1, 2.5, 5, or 10 ng/ml TGF-β2 for 48 h. *B,* the expression of TFPI2 and SMURF2 in hRGECs following treatment of 5 ng/ml TGF-β2 for 0, 12, 24, or 48 h. To explore the molecular mechanism of TGF-β2-induced TFPI2 expression, we next verified whether TFPI2 is a direct target gene of TGF-β/Smad signal. According to JASPAR prediction, TFPI2 is a potential target gene of SMAD2/3/4. *C,* the promoter activity of TFPI2 gene under TGF-β2 stimulation was detected by Dual-Luciferase Reporter Assay. *D,* SMAD4 was knocked down in hRGECs in the presence of TGF-β2, which was confirmed by Western blot. *E,* the expression of TFPI2 was detected in SMAD4-silencing cells. Data are shown as the mean ± SD (n = 3). *$p < 0.05$, **$p < 0.01$, ***$p < 0.001$. hRGEC, human renal glomerular endothelial cell; SMURF2, SMAD ubiquitination regulatory factor-2; TFP12, tissue factor pathway inhibitor 2; TGF-β, transforming growth factor beta.

CO-IP of endogenous TFPI2 with SMURF2 verified the interaction of TFPI2 and SMURF2 in hRGECs in the presence or absence of TGF-β2 (Fig. 10*A*). There were more immunocomplexes of TFPI2 and SMURF2 in the presence of TGF-β2, which could be attributed to TGF-β2-induced upregulation of SMURF2 (Fig. 7, *A* and *B*). The expression of TFPI2 and SMURF2 was found extensively in hRGECs and predominately in the nucleus (Fig. 10*B*). Double immunofluorescence revealed the colocalization of SMUIRF2 and TFPI2 in hRGECs in the absence or presence of TGF-β2. As expected, SMURF2 interacted with SMAD7 in hRGECs, which were evidenced by double immunofluorecence (Fig. 10*C*) and CO-IP analysis (Fig. 10*D*). In the absence of TGF-β2, both SMURF2 and SMAD7 were lowly expressed, and SMAD7 was found in the plasma membrane of the cell (Fig. 10*C*), presumably due to the binding with activated TGFBRs. Upon TGF-β2 stimulation, SMURF2, similar to SMAD7, was predominately expressed in the nucleus. In the absence of TFPI2, SMAD7 was found highly expressed in the nucleus and extensively interacted with SMURF2. Surprisingly, we found that overexpression of TFPI2 decreased SMAD7 expression, caused redistribution of SMURF2 to the outside the nucleus, and inhibited SMURF2/

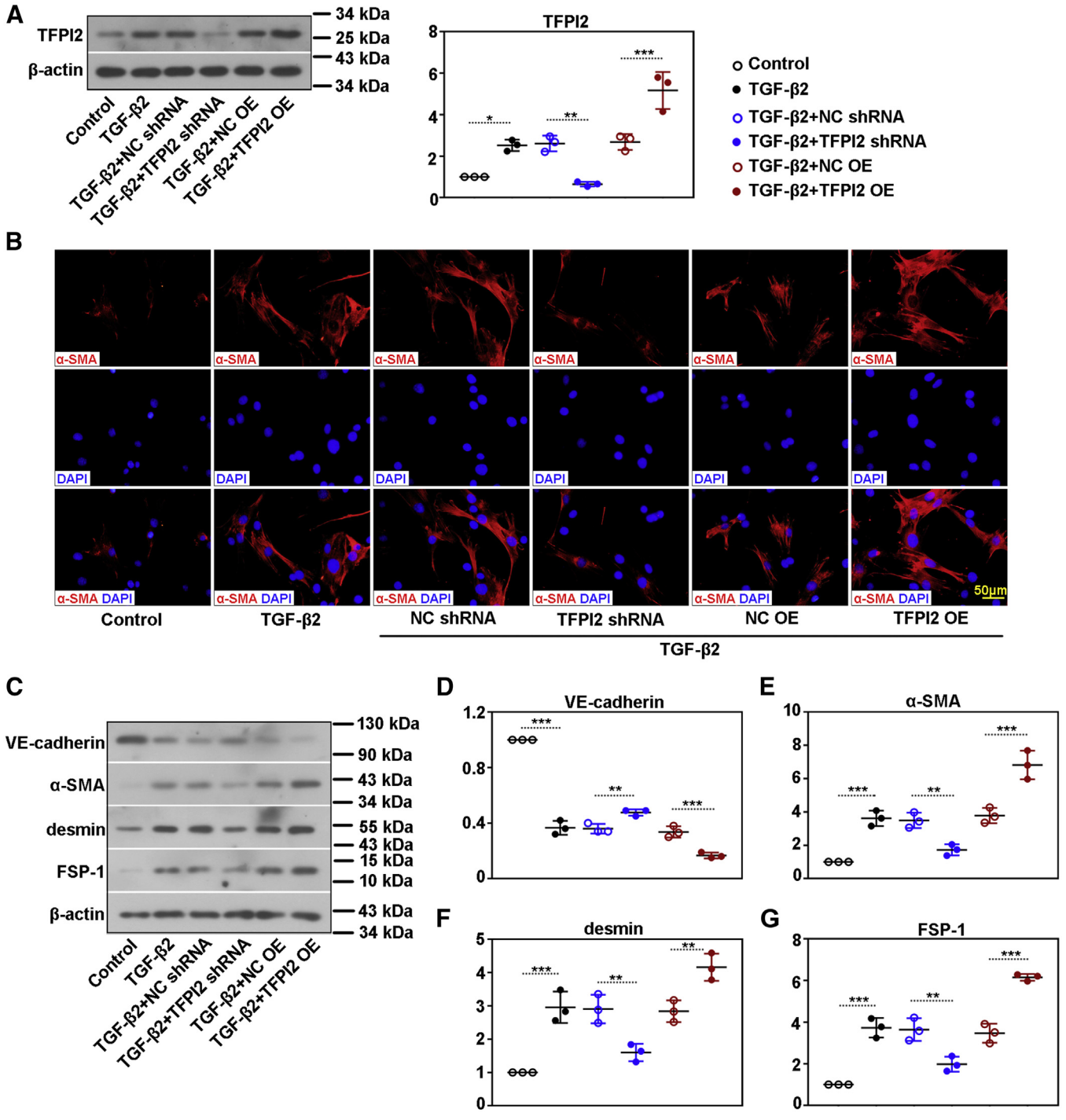

Figure 8. TFPI2 promotes TGF-β2-induced EndMT *in vitro*. TGF-β2 is considered as a potent inducer of EndMT. Human renal glomerular endothelial cells (hRGECs) were treated with 5 ng/ml TGF-β2 for 48 h to induce EndMT. *A,* Western blotting analysis revealed TGF-β2-induced TFPI2 expression as well as adenovirus-mediated TFPI2 knockdown (TFPI2 shRNA) and TFPI2 overexpression (TFPI2 OE) *in vitro*. *B,* immunofluorescent staining for α-SMA in hRGECs. *C,* Western blotting and semiquantitative analysis of (*D*) VE-cadherin, (*E*) α-SMA, (*F*) desmin, and (*G*) FSP-1 expression. Data are shown as the mean ± SD (n = 3). $^{*}p < 0.5$, $^{**}p < 0.01$, $^{***}p < 0.001$. EndMT, endothelial–mesenchymal transition; hRGEC, human renal glomerular endothelial cell; TFP12, tissue factor pathway inhibitor 2.

SMAD7 complex formation. Ubiquitination assay indicated that loss of TFPI2 enhanced TGFBR1/2-ubiquitin binding and overexpression of TFPI2 suppressed ubiquitylated TGFBR1/2 in hRGECs under TGF-β2 stimulation (Fig. 9, *E* and *F*). Taken together, TFPI2-induced TGF-β/Smad activation might be attributed to its inhibition on SMURF2/SMAD7 interaction.

Discussion

Diabetes is a global health problem and causes multiple comorbidities (such as liver disease and cancer) and complications (such as diabetic foot, heart attack, and DN) (33). Currently, DN is the worldwide common cause of end-stage renal disease that requires kidney replacement (34). Tissue

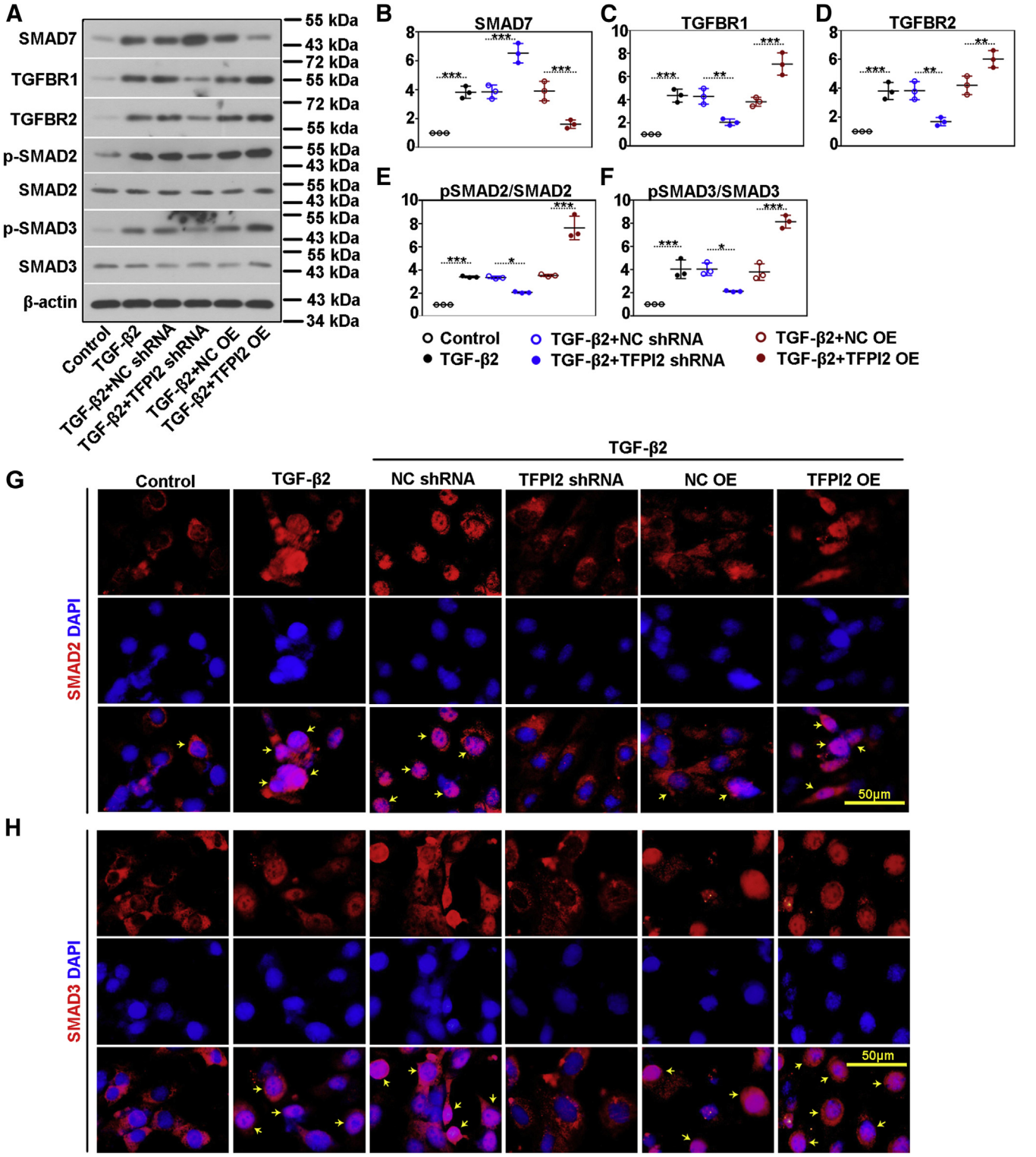

Figure 9. TFPI2 promotes TGF-β/Smad signaling activation. Human renal glomerular endothelial cells (hRGECs) were infected with adenovirus encoding shRNA targeting TFPI2 (TFPI2 shRNA) or overexpressing TFPI2 (TFPI2 OE), followed by stimulation of 5 ng/ml TGF-β2 for 48 h. *A,* the expression of SMAD7, TGFBR1, TGFBR2, SMAD2/3, and phospho-SMAD2/3 (p-SMAD2/3) was determined by Western blot. Semiquantitative analysis of (*B*) SMAD7, (*C*) TGFBR1, and (*D*) TGFBR2, as well as (*E* and *F*) the ratio of p-SMAD2/3 to SMAD2/3. *G* and *H,* immunofluorescent staining of SMAD2/3 in hRGECs. *Yellow arrows* indicated nuclear translocation of SMAD2/3. Data are shown as the mean ± SD (n = 3). *$p < 0.05$, **$p < 0.01$, ***$p < 0.001$. TGF-β, transforming growth factor beta; TFP12, tissue factor pathway inhibitor 2.

fibrosis is one of the prominent pathological features of DN, due to an increase in cellular glucose uptake (35). In this study, we used two different mouse models of T2DM to study DN *in vivo*: STZ-induced diabetic C57BL/6 mice and genetically diabetic db/db mice. They are both common experimental DN models (36, 37). As expect, both

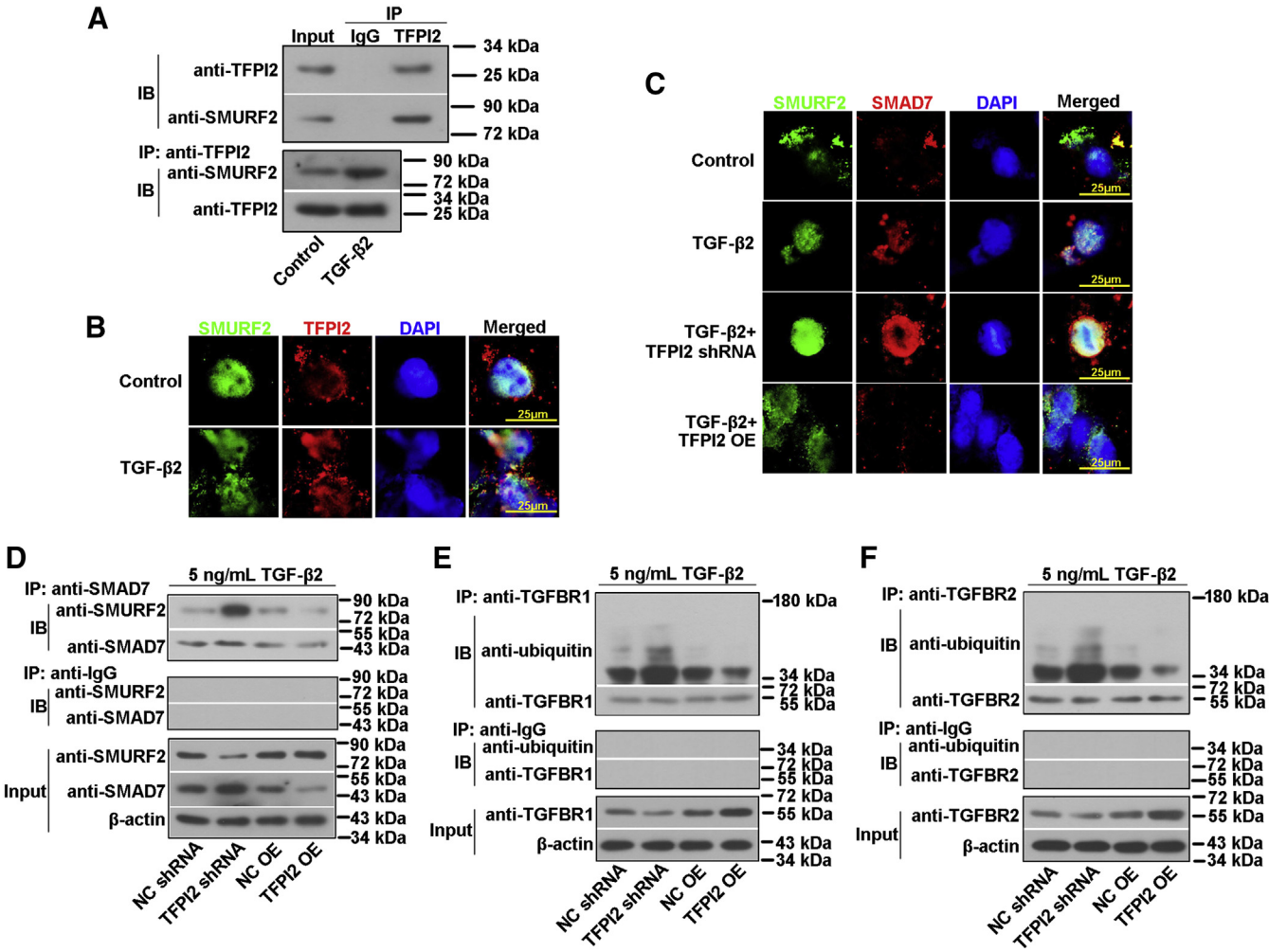

Figure 10. TFPI2 inhibits SMURF2/SMAD7 complex formation and thus regulates TGF-β signaling. To better understanding the molecular mechanism of TFPI2-mediated EndMT under TGF-β2 stimulation, all *in vitro* studies were performed using human renal glomerular endothelial cells (hRGECs) in the presence of TGF-β2 (5 ng/ml, 48 h). *A,* CO-IP of endogenous TFPI2 with SMURF2 in hRGECs in the presence or absence of TGF-β2. *B,* double immunofluorescence for colocalization of TFPI2 and SMURF2 in hRGECs under confocal microscopy. *C,* double immunofluorescence for colocalization of SMURF2 and SMAD7 in the presence or absence of TGF-β2 or TFPI2. *D,* CO-IP of endogenous SMAD7 with SMURF2 in hRGECs under TGF-β2 stimulation. *E* and *F,* ubiquitination assay showing the ubiquitylated TGFBR1 or TGFBR2 in TFPI2-silencing and -overexpressing hRGECs. CO-IP, coimmunoprecipitation; EndMT, endothelial–mesenchymal transition; hRGEC, human renal glomerular endothelial cell; SMURF2, SMAD ubiquitination regulatory factor-2; TGF-β, transforming growth factor beta; TFP12, tissue factor pathway inhibitor 2.

established mouse models of T2DM developed clinical and molecular features of human DN. Serum levels of blood glucose, BUN, creatinine, NGAL, and periostin, as well as 24-h urine protein content, were abnormally augmented in model mice. Tubulointerstitial fibrosis developed in renal cortex representing a key lesion of progressive DN as previously reported (36, 37). Importantly, mice developed experimental DN accompanied with abnormal upregulation of TFPI2 in renal cortex. However, the contribution of TFPI2 to DN has not been unveiled yet. TFPI2 is mainly expressed by endothelial cells (22). Endothelial cells derived from blood vessels take primary responsibility for maintaining vascular homeostasis (38). Endothelial dysfunction is a primary lesion in diabetes, resulting in multiple vascular complications (39). We speculated that TFPI2 might be involved in the pathogenesis of DN through regulating endothelial cell injury.

Increasing studies suggest that glomerular endothelial cell injury predominately contributes to the development and progression of DN (40). Dysfunction of hRGECs is considered to involve in microalbuminuria, an early event in DN (40). *In vitro*, high-glucose-induced hRGEC injury was observed by augmented cell apoptosis, which was suppressed by knockdown of TFPI2 and aggravated by overexpression of TFPI2. *In vivo*, TFPI2 deficiency efficiently suppressed hyperglycemia-mediated renal apoptosis and thus protected against rental dysfunction and DN development (41). Recent studies suggest a cross talk of hRGECs with other glomerular cells, such as mesangial cells and podocytes, in the pathogenesis of DN (40). Mesangial cell apoptosis resulted from high-glucose deteriorated DN (42). More investigations are needed to answer that whether TFPI2 contributes to the progression of DN through regulating the communication of hRGECs with other glomerular cells.

EndMT is closely implicated in the progression of human diabetes-associated fibrotic disorders, including DN. EndMT causes the conversion of endothelial cells into mesenchymal cells and further switching the phenotype to myofibroblasts, leading to tissue fibrosis (14, 43). Under pathological conditions such as hyperglycemia, this unrestrained activation results in excess ECM deposition (44). When exposed to high glucose, endothelial cells undergo EndMT and shift toward mesenchymal phenotype (45). In the setting of EndMT, endothelial cells acquire the ability to synthesize ECM protein accompanied by loss of endothelial markers such as VE-cadherin and CD31 and gain of mesenchymal markers such as α-SMA, desmin, and FSP-1 (46). Liu *et al*. evidenced that high glucose induced EndMT through TGF-β/Smad signaling by decreasing the phosphorylation of SMAD2/3 and increasing SMAD7 expression, which altered human umbilical vein endothelial cell function (47). Thus, in diabetic complications, EndMT appears to account for endothelial cell dysfunction and the progression into DN. The contribution of EndMT to myofibroblast accumulation and fibrosis indicates the therapeutic potential by targeting EndMT against DN. Knockdown of TFPI2 seemed to greatly retard EndMT process in renal cortex as observed by increased expression of endothelial markers and decreased expression of mesenchymal markers. There was a reduction in renal fibrosis in diabetic mice with TFPI2 deficiency. Thus, the involvement of TFPI2 in renal fibrosis in DN might be achieved through regulating EndMT process.

TGF-β is a key driver of EndMT, and all three TGF-β isoforms (TGF-β1, TGF-β2, and TGF-β3) have been shown to induce EndMT in human microvascular endothelial cells (48). The effect of TGF-β2 on inducing EndMT was found to be the most pronounced, and treatment with TGF-β1 and TGF-β3 was considered as the secondary effects through TGF-β2 secretion. Thus, TGF-β2 was used as the inducer of EndMT (49). In the present study, we observed TGF-β2-induced EndMT in hRGECs and their phenotype switching toward mesenchymal cells, as evidenced by increased expression of mesenchymal markers α-SMA, desmin, and FSP-1 and decreased expression of VE-cadherin. Sabbineni *et al*. observed that TGF-β2 induced activation of SMAD2/3 and p38 MAPK signaling, which were both involved in promoting EndMT *in vitro* (48). Zeng and coworkers reported that TGF-β2-mediated SMAD2/3 signaling activation led to EndMT (50). TFPI2 was preliminarily verified as a downstream target gene of TGF-β/Smad signaling. The promoter activity of TFPI2 gene and its protein expression were increased in the presence of TGF-β2. Adenovirus-mediated TFPI2 knockdown suppressed TGF-β2-induced EndMT in hRGECs, while TFPI2 overexpression promoted it. The effect of TGF-β1 or TGF-β3 on EndMT in hRGECs is unknown, and whether they exert similar effects as TGF-β2 does requires further exploration. TGF-β signals through forming complexes with transmembrane Ser/Thr kinase receptors (TGFBR1/2), in which the activated TGF-β receptors propagated signals to the downstream Smad signaling pathway (51, 52). SMAD2/3 proteins are specifically regulated by TGF-β receptors, and their activation enhances the progression of fibrosis. SMAD2 deficiency reduced fibrosis and EMT in STZ-induced mouse model of DN (53). Depletion of SMAD3 prevented renal fibrosis in db/db mice (54). In hRGECs, TGF-β2 increased the phosphorylation of SMAD2 and SMAD3 and their translocation into nucleus, indicating the activation of its downstream SMAD2/3 signaling. Upon TGF-β2 stimulation, inhibition of TFPI2 reduced the expression of TGFBR1/2 as well as the phosphorylation of SMAD2/3. In contrast, enforced expression of TFPI2 had opposite effects. Thus, TFPI2 might promote the activation of Smad-dependent TGF-β signaling. SMAD7 is not only a regulator but also a cross-talk mediator of TGF-β signaling (55). On the one hand, SMAD7 is a direct target gene for TGF-β/Smad signal (55). In the present, the expression of SMAD7 was increased in hRGECs upon TGF-β2 stimulation. On the other hand, SMAD7 is a well-established negative regulator of TGF-β signaling (56). Interestingly, SMAD7 expression was found further increased by overexpression of TFPI2, while decreased by knockdown of TFPI2 in the presence of TGF-β2. The negative regulation of TFPI2 on SMAD7 expression suggested the potential inhibition of TFPI2 on SMAD7-mediated inhibition of TGF-β signaling, which indirectly supported TFPI2-induced activation of TGF-β/Smad signaling. However, the underlying mechanism of TFPI2-mediated downregulation of SMAD7 is not unveiled in the present study. The effect of TFPI2 on SMAD7 expression and function as well as the cross talk with TGF-β/Smad signaling requires further exploration. Based on the current study, we demonstrated that TFPI2-mediated activation of TGF-β/Smad signaling might account for its regulation on EndMT and fibrosis in DN.

SMAD ubiquitination regulatory factor-2 (SMURF2) is a HECT domain E3 ubiquitin-protein ligases that recruits substrates and specifies targeted proteins for ubiquitination and degradation (57). SMURF2-mediated ubiquitin proteasome system is involved in the degradation of various cellular proteins, including SMADs (58). Lin *et al*. demonstrated that SMURF2 negatively regulated SMAD2 signal transduction by proteasome-dependent pathway in TGF-β signaling (59). Tang *et al*. indicated that SMURF2 inhibited TGF-β signaling by decreasing SMAD3 activity *via* inducing mono-ubiquitination of SMAD3 (60). Thus, SMURF2 plays an important role in the regulation of TGF-β signaling pathway (61, 62). Besides, TGF-β has been implicated in the transcriptional induction of SMURF2 and promoting SMURF2 expression (63). In hRGECs, TGF-β2 stimulation induced the expression of TFPI2 and SMURF2 at a time- and concentration-dependent manner. TFPI2 and SMURF2 were found extensively expressed in hRGECs and predominately in the nucleus, and their interaction was verified in this study. The localization of TFPI2 or SMURF2 was not altered in the presence of TGF-β2. A previous study has reported that SMURF2 is mainly expressed in the nucleus, and TGFBR complex coexpression has no effect on its localization (32). To better understanding the molecular mechanism of TFPI2-mediated EndMT induced by TGF-β2, we performed all *in vitro* studies in the presence of TGF-β2. Interestingly, the

formation of TFPI2-SMURF2 immunocomplexes was increased in the presence of TGF-β2, which might be partially attributed to TGF-β2-induced upregulation of TFPI2 and SMURF2 expression. Whether and how TGF-β signal in turns affects TFPI2 localization or SMURF2/SMAD7 interaction deserves more studies. Overall, our current data validated the interaction between TFPI2 and SMURF2 and implied that TFPI2 might function through regulating SMURF2.

SMAD7 belongs to the inhibitory Smads and negatively regulates TGF-β signaling through interacting with TFGBR (64). Importantly, SMAD7 is able to recruit SMURF2 to TGF-β receptors to mediate their ubiquitination and degradation, leading to suppression of TGF-β signaling (32, 65). As expected, SMURF2 interacted with SMAD7 in hRGECs under TGF-β2 stimulation as previously described (32). We further explored the potential regulation of TFPI2 on SMURF2-SMAD7 interaction and TGF-β/Smad signaling. SMAD7 and SMURF2 have been reported as downstream target genes of TGF-β/Smad signal (55, 63). In the presence of TGF-β2, the expression of SMAD7 and SMURF2 was increased in hRGECs. Notably, TFPI2 knockdown increased SMAD7 expression and promoted the formation of SMURF2-SMAD7 complex, while its overexpression decreased SMAD7 expression and inhibited SMURF2-SMAD7 combination. Interestingly, we found that SMURF2 was predominately outside the nucleus in the presence of TFPI2. We presumed that TFPI2 overexpression might export SMURF2 from the nucleus and inhibited its binding to SMAD7. Peter *et al*. reported that SMAD7 could interact with SMURF2 and recruit it to the cell plasma membrane and TGFBR complex, leading to TGFBRs degradation (32). Upon TFPI2 overexpression, SMURF2 failed to interact with SMAD7 and target TGFBRs for degradation. However, these presumptions need in-depth confirmation in the future study. The effect of TFPI2 on SMAD7 expression and function and the underlying mechanism require further study as well. However, our results clearly evidenced that TFPI2 overexpression reduced the colocalization of SMURF2 and SMAD7 and inhibited SMURF2/Smad7 complex formation in hRGECs under TGF-β2 stimulation. The regulation of TFPI2 on SMURF2-SMAD7 interaction and the underlying mechanisms deserve more investigation. It has been reported that SMAD7 interacts with SMURF2 and recruits it to the TGFBR complex, leading to SMURF2-mediated ubiquitination of SMAD7 and thus degradation of TGFBRs *via* the proteasome and lysosome pathways (32). In our study, TFPI2 was identified to interact with SMURF2. TFPI2 knockdown promoted SMURF2-SMAD7 interaction and induced ubiquitination and degradation of TGFBR1/2, and its overexpression exhibited opposite effects. Taken together with previous findings, we speculate that TFPI2 may inhibit SMURF2-SMAD7 interaction by binding to SMURF2 and thus prevent SMURF2 from targeting TGFBR1/2 *via* SMAD7-dependent recruitment, which causes subsequent activation of TGF-β/Smad signaling and leads to EndMT and fibrosis. A recent study showed that SMURF2 suppressed TGF-β-induced EMT by triggering the degradation of TGFBR1 (31). In agreement with previous findings, we demonstrate that the contribution of TFPI2 to TGF-β2-induced EndMT is partially attributed to its regulation on SMURF2-SMAD7 interaction.

In the present study, we found that (1) TFPI2 is a downstream target gene of TGF-β/Smad signal, and its expression was augmented in the presence of TGF-β2; (2) TFPI2 inhibited SMURF2-SMAD7 interaction and suppressed TGFBRs degradation, leading to TGF-β/Smad signaling activation; (3) TFPI2 promoted EndMT and fibrosis in DN. Taken together, our study provides clear evidence that TFPI2 regulates SMURF2/SMAD7 complex formation and TGF-β/Smad signaling and suggests that TFPI2 likely promotes TGF-β/SMAD2/3 signaling by inhibiting SMAD7-mediated recruitment of SMURF2 to TGFBR1/2 and consequent ubiquitination and degradation of TGFBR1/2 (Fig. 11). We fail to provide more details on the mechanism of how TFPI2 regulates SMURF2/SMAD7 interaction. Moreover, whether TFPI2-mediated TGF-β/Smad signaling regulates EndMT and fibrosis in DN remains to be established *in vivo*. In addition to the SMAD2/3 signaling pathway, TGF-β2 also induces EndMT and exerts its biological functions through non-Smad signal transduction pathways, such as MAPK (ERK and p38) (66, 67). Interestingly, the contribution of TGF-β/SMAD1/5 pathway to EndMT has been recently indicated (68, 69). The possibility that TFPI2 functions through other signaling pathway in addition to SMAD2/3 signal has not been established yet. The underlying mechanism of TFPI2 in TGF-β-induced EndMT is not fully unveiled and deserves further investigation. It is known that TFPI2 is synthesized by a variety of endothelial cells (22). The role of TFPI2 in endothelial cells derived from different blood vessels and its contribution to the progression of DN require an in-depth exploration. To further confirm the role of TFPI2 in DN and explore the underlying mechanisms, more studies, such as using other shRNAs targeting TFPI2 to avoid the off-target effect and overexpression of TFPI2, are needed to be performed *in vivo* and *in vitro* in the future.

In conclusion, we demonstrate that TFPI2 is highly expressed in renal cortex of diabetic mice and its inhibition attenuated cell apoptosis, renal fibrosis, and EndMT and thus improved renal function in experimental DN. *In vitro* studies further identified that TFPI2 promotes TGF-β/Smad signaling by intervening the interaction of SMURF2 with SMAD7 and consequent TGFBR1/2 ubiquitination and degradation. Having known the importance of TGF-β signaling pathway in EndMT and fibrotic process, we demonstrate that TFPI2 contributes to DN progression by promoting renal fibrosis and EndMT *via* regulating SMURF2/SMAD7-mediated TGF-β/Smad signaling pathway. These findings provide novel insights into the pathogenesis of DN and suggest a potential therapeutic approach to DN.

Experimental procedures

Animal experiments

Male C57BL/6 mice (Liaoning Changsheng Biotechnology), db/db and db/dm mice (Huafukang Biotechnology) were used in this study. All animal experiments were performed in accordance with the National Institutes of Health Guide for

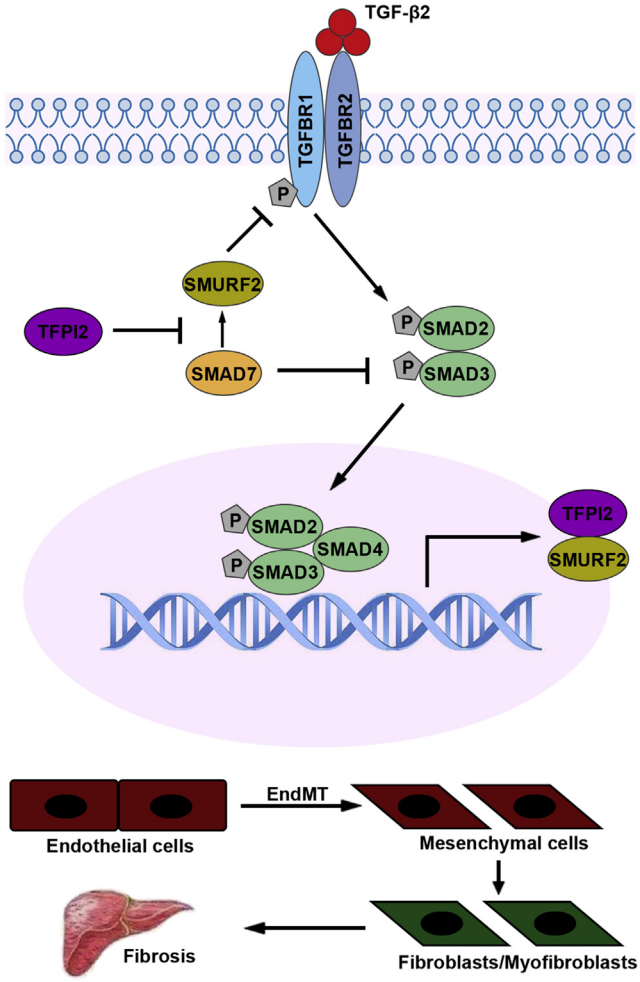

Figure 11. The potential mechanism underlying TFPI2-mediated EndMT and fibrosis in DN: involvement of TGF-β/Smad signaling. TFPI2, as a downstream target gene of TGF-β/Smad signal, is induced upon TGF-β2 stimulation. In the presence of TGF-β2, TFPI2 interacts with SMURF2 and inhibits SMURF2/SMAD7 interaction, and thus suppressing TGFBRs degradation, leading to Smads signaling activation. Subsequently, TFPI2-induced activation of TGF-β/Smad signaling promotes EndMT and renal fibrosis. EndMT, endothelial–mesenchymal transition; SMURF2, SMAD ubiquitination regulatory factor-2; TFP12, tissue factor pathway inhibitor 2; TGFBR, TGF-β receptor.

the Care and Use of Laboratory Animals and approved by the Committee Ethics of The First Affiliated Hospital of Harbin Medical University.

Two different mouse models of T2DM were established as Figure 1*B* and used as *in vivo* models of DN. C57BL/6 mice at 8–9 weeks of age were intraperitoneally injected with 50 mg/kg STZ (S17049, ShanghaiyuanyeBio-Technology) in citrate buffer (PH 4.5) for five consecutive days. The mice underwent fasting for 4 h before each injection. The control mice received same volume of citrate buffer in the same way. Three days after the last STZ injection, the development of diabetes was confirmed as the blood glucose level higher than 16.7 mM. The diabetic mice were intravenously injected with a single dose of AAV2 carrying TFPI2 shRNA or negative NC shRNA (1×10^{11} genome copies/mouse) at 2 weeks after the first STZ injection. Mice were sacrificed at 24 weeks after the first STZ injection, and the kidney, blood, and urine samples were collected. Genetically obese male C57BLKS-Leprdb/Leprdb (db/db) mice were commonly used as a mouse model of T2DM, and C57BLKS-Leprdb/+ (db/dm) mice served as nondiabetic controls. The db/db mice at 12 weeks of age were injected with AAV2-TFPI shRNA or NC shRNA (1×10^{11} genome copies/mouse) as previously described. At the age of 20 weeks, db/db or db/dm mice were sacrificed, and the kidney, blood, and urine samples were collected.

The body weight of each mouse was recorded weekly. At the end of the modeling, blood glucose of each mouse was measured 2 h after gavage administration of glucose solution (2 g/kg).

Serum index and urine protein measurements

The following commercial kits were used to detect serum indexes: BUN Assay Kit (#C013-2), Creatinine Assay Kit (#C011-1), and Urine protein Test Kit (#C035-2) from Nanjing Jiancheng Bioengineering Institute, and Mouse NGAL ELISA Kit (#EM1232) and Mouse POSTIN/OSF-2 (Periostin) ELISA Kit (#EM0290) from Wuhan Fine Biotech. All detections were performed in accordance with the respective manufacturer's instruction.

Real-time polymerase chain reaction (real-time PCR)

Total RNA was extracted from kidney tissues with the use of TRIpure lysis buffer (#RP1001; BioTeke), and RNA concentration was determined using NANO 2000 (Thermo Fisher Scientific). RNA samples were reversely transcribed into cDNA with reverse transcriptase BeyoRT II M-MLV (#D7160L; Beyotime). Then PCR reaction was carried out in a final volume of 20 μl, containing 1 μl of cDNA, 0.5 μl of forward primer (10 μM), 0.5 μl of reversed primer (10 μM), 0.3 μl of SYBR GREEN (#SY1020; Solarbio), 10 μl of 2 × Taq PCR Master Mix (#PC1150, Solarbio), and ddH_2O. The primer sequences were as following: TFPI2 forward, 5′-TCCGTTCTTGGTCTCACT-3′; TFPI2 reverse, 5′-AGCAGCCTCCATAGTTGA-3′; β-actin forward, 5′-CTGTGCCCATCTACGAGGGCTAT-3′; β-actin reverse, 5′-TTTGATGTCACGCACGATTTCC-3′. β-actin was used as an internal reference gene to normalize the expression of TFPI2. Quantification of TFPI2 by real-time PCR was performed on the ExicyclerTM 96 Real-Time Quantification Thermal Block (Bioneer) using $2^{-\triangle\triangle Ct}$ method. Each individual experiment was repeated in triplicate, and the mean value of the controls was arbitrarily set as 100%.

Western blot assay

Total protein was extracted from kidney tissue or cell samples using RIPA lysis buffer (#P0013B, Beyotime) containing 1% phenylmethylsulfonyl fluoride (PMSF) (#ST506, Beyotime), and protein concentration was determined with BCA Protein Assay kit (#P0009, Beyotime). Protein samples were separated by SDS-PAGE and transferred onto polyvinyl difluoride (PVDF) membranes (#LC2005, Thermo Fisher Scientific,). The blots were blocked with 5% bovine serum albumin (BSA) (#BS043; Biosharp) for 1 h and probed with primary antibody at 1:1000 or

1:2000 dilution at 4 °C overnight and then secondary antibody at 1:10,000 dilution at 37 °C for 40 min. The primary antibodies were as following: anti-TFPI2 (#A03697-1; Boster, Wuhan, China), anti-SMAD4 (#A19116; ABclonal), anti-SMURF2 (#DF7683; Affinity Biosciences, Jiangsu, China), anti-pro/cleaved caspase 3 (#A19654; ABclonal), anti-pro/cleaved caspase 7 (#12827; Cell Signaling Technology), anti-VE-cadherin (#AF6265, Affinity), anti- α-SMA (#ab7817; Abcam), anti-desmin (#A3736, ABclonal), anti-FSP-1 (#A1631, ABclonal), anti-SMAD7 (#AF5147, Affinity), anti-TGFBR1 (#AF5347, Affinity), anti-TGFBR2 (#AF5449, Affinity), anti-SMAD2 (#AF6449, Affinity), anti-p-SMAD2 (#AF3449, Affinity), anti-SMAD3 (#AF6362, Affinity), anti-p-SMAD3 (#AF8315, Affinity), anti-ubiquitin (#A19686, ABclonal) and anti-β-actin (#60008-1-Ig; Proteintech Group, Rosemont, IL, USA). β-actin served as an internal reference gene. The secondary antibodies include horseradish peroxidase (HRP)-conjugated goat anti-rabbit IgG (#SA00001-2, Proteintech) and goat anti-mouse IgG (#SA00001-1, Proteintech). For detection, the blots were incubated with ECL luminescence reagent (#E003; SevenSea biotech) for 5 min in the dark. The protein band density was analyzed by a Gel-Pro Analyzer software.

Immunohistochemistry

Paraformaldehyde-fixed and paraffin-embedded kidney tissues were sectioned into 5-μm thickness. The sections were deparaffinized with xylene and ethanol and subjected to antigen retrieval solution by boiling for 10 min. The endogenous peroxidase was blocked with 3% H_2O_2 (#10011218, Sinopharm) for 15 min. Then the sections were incubated with normal goat serum (#SL038, Solarbio) for 15 min, anti-TFPI2 (#A03697-1, Boster) at 1:50 dilution at 4 °C overnight and HRP-conjugated goat anti-rabbit IgG (#31460, Thermo Fisher) at 1:500 dilution at 37 °C for 1 h and then developed by diaminobenzidine (DAB) (#DA1010, Solarbio). After counterstaining with hematoxylin (#H8070, Solarbio), the sections were observed under a light microscopy at a magnification of 400×.

PAS staining was used for detection of glycogen synthesis in kidney tissues. Briefly, the sections were treated with PAS staining solution (#DG0005; Leagene Biotechnology) for 15 min and counterstained with hematoxylin for 2 min. Masson staining was performed for evaluation of kidney fibrosis. Briefly, kidney tissue sections were treated with hematoxylin for nuclear staining and Li Chunhong acid fuchsin staining solution (#p8330, ##71019360, Sinopharm) and restained with aniline blue. The samples were observed under a light microscopy at a magnification of 200×.

Cell culture and treatments

hRGECs purchased from Hunan Fenghui Biotechnology were cultured under 5% CO_2 at 37 °C in an endothelial cell medium (#1001; Sciencell) containing 5.5 mM glucose. Cells were identified by positive immunolabeling with CD31 as previously described. Loss-of-function and gain-of function studies for TFPI2 were performed *in vitro* using adenovirus deliver system. Cells were infected with recombinant adenovirus expressing TFPI2 shRNA or TFPI2 OE. After 24 h, the cell culture medium was replaced by fresh endothelial cell medium supplemented with 30 mM glucose or isotonic mannitol as a contrast and cultured for 48 h.

For induction of EndMT *in vitro*, recombinant human TGF-β2 (#MA0624, Dalian Meilun Biotech) was added to the cell culture medium at a concentration of 0, 1, 2.5, 5, or 10 ng/ml and cultured for 0, 12, 24, or 48 h.

Immunofluorescent staining

TUNEL staining was performed on kidney tissue sections with the *In Situ* Cell Death Detection Kit (#11684795910; Roche) according to the manufacturer's instruction and analyzed under a fluorescent microscopy at a magnification of 400×. For double immunofluoresence staining, kidney tissue sections were treated with anti-TFPI2 (#03697-1, Boster) at 1:50 dilution and anti-CD31 (#ab24590, Abcam) at 1:200 dilution followed by corresponding secondary antibodies including fluorescein isothiocyanate (FITC)-labeled goat anti-rabbit IgG (#A0562, Beyotime) and Cy3-labeled goat anti-mouse IgG (#A0521, Beyotime) at 1:200 dilution.

Cells grown on slides were fixed in 4% paraformaldehyde (#80096618, Sinopharm) for 15 min and incubated with 0.1% tritonX-100 (#ST795, Beyotime) for 30 min. After blocking with normal goat serum (#SL038, Solarbio) for 15 min, cells were incubated with primary antibody in appropriate dilution at 4 °C overnight and then secondary antibody at 37 °C for 40 min. The primary antibodies include anti-CD31 (#ab24590, Abcam), anti-α-SMA (#ab7871, Abcam), anti-SMAD2 (#A7699, Abclonal), and anti-SMAD3 (#A16913, Abclonal). The secondary antibodies include Cy3-labeled goat anti-rabbit IgG (#A0516, Beyotime) and goat anti-mouse (#A0512, Beyotime). DAPI (#D106471; Aladdin) was used for nuclear counterstaining. Slides were mounted with anti-fluorescence quenching agent (#S2100, Solarbio) and analyzed under a fluorescence microscopy at a magnification of 400×. For double immunofluorescence staining, cells were probed with anti-TFPI2 (#sc-48380; Santa Cruz), anti-SMURF2 (#DF7683, Affinity) at 1:100 dilution or anti-SMAD7 (#sc-101152, Santa Cruz) at 1:50 dilution and hybridized with Cy3-labeled goat anti-mouse IgG (#A0521, Beyotime) or FITC-labeled goat anti-rabbit IgG (#A0562, Beyotime) at 1:200 dilution as previously described. The samples were analyzed under laser scanning confocal microscopy at a magnification of 600×.

Flow cytometry for cell apoptosis

Cell apoptosis was detected with Annexin-FITC Apoptosis Detection Kit (#C1062, Beyoitme). Briefly, cells were treated with Annexin-FITC and propidium Iodide (PI) according to manufacturer's instruction. Flow cytometry was carried out according to the standard procedure.

Dual-luciferase reporter assay

The promoter activity of TFPI2 gene under TGF-β2 stimulation was assessed with the dual-luciferase reporter assay system (#KGAF040; KeyGEN). The human TFPI2 gene promoter sequences (–2000 ∼ +30 bp) were amplified by PCR, and TFPI2 gene promoter was inserted into the luciferase reporter gene vector pGL3-basic (pGL3-TFPI2). The empty vector pGL3-basic was used as a control. The constructed TFPI2 gene promoter luciferase reporter plasmids or the control plasmids were transfected into HEK293 cells using Lipofectamine 2000 transfection reagent (#11668019; Invitrogen). Forty-eight hours after transfection, cells were stimulated with different concentrations of TGF-β2 for 6 h and then subjected to luciferase activity detection. The gene promoter activity was calculated as the ratio of Firefly/Renilla luciferase activity.

Coimmunoprecipitation (CO-IP)

Cells were lysed with cell lysis buffer (#P0013, Beyotime). Whole cell lysates were obtained after centrifugation, and protein concentration was determined. The protein extracts were diluted to 1 μg/μl in phosphate buffer saline (PBS) and then incubated with 1 μg of the indicated antibody and 60 μl protein A agarose beads for 2 h at 4 °C. The antibodies for IP include anti-TFPI2 (#sc-48380; Santa Cruz), anti-SMAD7 (#sc-101152, Santa Cruz), anti-TGFBR1 (#sc-518018, Santa Cruz), and anti-TGFBR2 (#sc-17792, Santa Cruz). IgG was used as a negative control. Immunocomplexes obtained by centrifugation were separated by SDS-PAGE, and immunoblotting was performed as previously described.

Statistic analysis

All data are shown as the mean ± SD of at least three independent experiments. Statistical analysis was performed using a two-tailed unpaired student's *t* test for two groups and a one-way analysis of variance (ANOVA) for more than two groups ($^{*}p < 0.05$, $^{**}p < 0.01$, $^{***}p < 0.001$).

Ethics approval

All animal studies were approved by the ethics committee of The First Affiliated Hospital of Harbin Medical University.

Data availability

The data that support the findings of this study are available from the corresponding author upon reasonable request.

Acknowledgment—This research was funded by the Youth Project of National Natural Science Foundation of China (No. 81600629) and the Surface Project of National Natural Science Foundation of China (No. 81671383).

Author contributions—G. G. and H. H. conceptualization; G. G., J. X., and Y. D. data curation; J. X. and Y. D. formal analysis; G. G. and H. H. methodology; Y. D. software; H. H. supervision; G. G., writing—original draft; J. X. writing—reviewing and editing.

Conflict of interest—The authors declare that they have no conflict of interests with the contents of this article.

Abbreviations—The abbreviations used are: AAV, adeno-associated virus; BUN, blood urea nitrogen; DN, diabetic nephropathy; ECM, extracellular matrix; EMT, epithelial–mesenchymal transition; EndMT, endothelial–mesenchymal transition; GEO, Gene Expression Omnibus; hRGEC, human renal glomerular endothelial cell; NGAL, neutrophil gelatinase-associated lipocalin; SMURF2, SMAD ubiquitination regulatory factor-2; STZ, streptozotocin; TGF-β, transforming growth factor beta; TFP12, tissue factor pathway inhibitor 2.

References

1. Reutens, A. T. (2013) Epidemiology of diabetic kidney disease. *Med. Clin. North Am.* **97**, 1–18
2. Thomas, B. (2019) The global burden of diabetic kidney disease: Time trends and gender gaps. *Curr. Diab. Rep.* **19**, 18
3. Zhang, L., Long, J., Jiang, W., Shi, Y., He, X., Zhou, Z., Li, Y., Yeung, R. O., Wang, J., Matsushita, K., Coresh, J., Zhao, M., and Wang, H. (2016) Trends in chronic kidney disease in China. *N. Engl. J. Med.* **375**, 905–906
4. Afkarian, M., Sachs, M. C., Kestenbaum, B., Hirsch, I. B., Tuttle, K. R., Himmelfarb, J., and de Boer, I. H. (2013) Kidney disease and increased mortality risk in type 2 diabetes. *J. Am. Soc. Nephrol.* **24**, 302–308
5. de Boer, I. H., Sun, W., Cleary, P. A., Lachin, J. M., Molitch, M. E., Steffes, M. W., and Zinman, B. (2011) Intensive diabetes therapy and glomerular filtration rate in type 1 diabetes. *N. Engl. J. Med.* **365**, 2366–2376
6. Pedone, E., Laurenzi, A., Allora, A., Bolla, A. M., and Caretto, A. (2020) Insulin pump therapy and continuous glucose monitoring in adults with type 2 diabetes: Where are we now? *Explor. Med.* **1**, 314–330
7. Alicic, R. Z., Rooney, M. T., and Tuttle, K. R. (2017) Diabetic kidney disease: Challenges, progress, and possibilities. *Clin. J. Am. Soc. Nephrol.* **12**, 2032–2045
8. Kawanami, D., Matoba, K., and Utsunomiya, K. (2016) Signaling pathways in diabetic nephropathy. *Histol. Histopathol.* **31**, 1059–1067
9. Zeng, L. F., Xiao, Y., and Sun, L. (2019) A glimpse of the mechanisms related to renal fibrosis in diabetic nephropathy. *Adv. Exp. Med. Biol.* **1165**, 49–79
10. Yuan, Q., Tan, R. J., and Liu, Y. (2019) Myofibroblast in kidney fibrosis: Origin, activation, and regulation. *Adv. Exp. Med. Biol.* **1165**, 253–283
11. Sun, Y. B., Qu, X., Caruana, G., and Li, J. (2016) The origin of renal fibroblasts/myofibroblasts and the signals that trigger fibrosis. *Differ. Res. Biol. Divers.* **92**, 102–107
12. Li, J., and Bertram, J. F. (2010) Review: Endothelial-myofibroblast transition, a new player in diabetic renal fibrosis. *Nephrology (Carlton)* **15**, 507–512
13. Piera-Velazquez, S., Li, Z., and Jimenez, S. A. (2011) Role of endothelial-mesenchymal transition (EndoMT) in the pathogenesis of fibrotic disorders. *Am. J. Pathol.* **179**, 1074–1080
14. Zeisberg, E. M., Potenta, S. E., Sugimoto, H., Zeisberg, M., and Kalluri, R. (2008) Fibroblasts in kidney fibrosis emerge via endothelial-to-mesenchymal transition. *J. Am. Soc. Nephrol.* **19**, 2282–2287
15. He, J., Xu, Y., Koya, D., and Kanasaki, K. (2013) Role of the endothelial-to-mesenchymal transition in renal fibrosis of chronic kidney disease. *Clin. Exp. Nephrol.* **17**, 488–497
16. Kang, Y. S., Li, Y., Dai, C., Kiss, L. P., Wu, C., and Liu, Y. (2010) Inhibition of integrin-linked kinase blocks podocyte epithelial-mesenchymal transition and ameliorates proteinuria. *Kidney Int.* **78**, 363–373
17. Kanasaki, K., Shi, S., Kanasaki, M., He, J., Nagai, T., Nakamura, Y., Ishigaki, Y., Kitada, M., Srivastava, S. P., and Koya, D. (2014) Linagliptin-mediated DPP-4 inhibition ameliorates kidney fibrosis in streptozotocin-induced diabetic mice by inhibiting endothelial-to-mesenchymal transition in a therapeutic regimen. *Diabetes* **63**, 2120–2131
18. Pardali, E., Sanchez-Duffhues, G., Gomez-Puerto, M. C., and Ten Dijke, P. (2017) TGF-β-induced endothelial-mesenchymal transition in fibrotic diseases. *Int. J. Mol. Sci.* **18**, 2157

19. Okazaki, Y., Yamasaki, Y., Uchida, H. A., Okamoto, K., Satoh, M., Maruyama, K., Maeshima, Y., Sugiyama, H., Sugaya, T., Kashihara, N., and Makino, H. (2007) Enhanced TGF-beta/Smad signaling in the early stage of diabetic nephropathy is independent of the AT1a receptor. *Clin. Exp. Nephrol.* **11**, 77–87
20. Yamamoto, T., Nakamura, T., Noble, N. A., Ruoslahti, E., and Border, W. A. (1993) Expression of transforming growth factor beta is elevated in human and experimental diabetic nephropathy. *Proc. Natl. Acad. Sci. U. S. A.* **90**, 1814–1818
21. Derynck, R., and Zhang, Y. E. (2003) Smad-dependent and Smad-independent pathways in TGF-beta family signalling. *Nature* **425**, 577–584
22. Iino, M., Foster, D. C., and Kisiel, W. (1998) Quantification and characterization of human endothelial cell-derived tissue factor pathway inhibitor-2. *Arterioscler. Thromb. Vasc. Biol.* **18**, 40–46
23. Miyagi, Y., Koshikawa, N., Yasumitsu, H., Miyagi, E., Hirahara, F., Aoki, I., Misugi, K., Umeda, M., and Miyazaki, K. (1994) cDNA cloning and mRNA expression of a serine proteinase inhibitor secreted by cancer cells: identification as placental protein 5 and tissue factor pathway inhibitor-2. *J. Biochem.* **116**, 939–942
24. Wojtukiewicz, M. Z., Sierko, E., Zimnoch, L., Kozlowski, L., and Kisiel, W. (2003) Immunohistochemical localization of tissue factor pathway inhibitor-2 in human tumor tissue. *Thromb. Haemost.* **90**, 140–146
25. Sierko, E., Wojtukiewicz, M. Z., and Kisiel, W. (2007) The role of tissue factor pathway inhibitor-2 in cancer biology. *Semin. Thromb. Hemost.* **33**, 653–659
26. Kempaiah, P., and Kisiel, W. (2008) Human tissue factor pathway inhibitor-2 induces caspase-mediated apoptosis in a human fibrosarcoma cell line. *Apoptosis* **13**, 702–715
27. Ivanciu, L., Gerard, R. D., Tang, H., Lupu, F., and Lupu, C. (2007) Adenovirus-mediated expression of tissue factor pathway inhibitor-2 inhibits endothelial cell migration and angiogenesis. *Arterioscler. Thromb. Vasc. Biol.* **27**, 310–316
28. Lin, Y. F., Zhang, N., Guo, H. S., Kong, D. S., Jiang, T., Liang, W., Zhao, Z. H., Tang, Q. Q., and Ma, D. (2007) Recombinant tissue factor pathway inhibitor induces apoptosis in cultured rat mesangial cells via its Kunitz-3 domain and C-terminal through inhibiting PI3-kinase/Akt pathway. *Apoptosis* **12**, 2163–2173
29. Liang, W., Cheng, J., Liu, R., Wang, J., Mu, J., Wang, Q., Wang, H., and Ma, D. (2009) Peptide corresponding to the C terminus of tissue factor pathway inhibitor inhibits mesangial cell proliferation and activation in vivo. *Peptides* **30**, 2330–2336
30. Wang, Z., Han, Z., Tao, J., Wang, J., Liu, X., Zhou, W., Xu, Z., Zhao, C., Wang, Z., Tan, R., and Gu, M. (2017) Role of endothelial-to-mesenchymal transition induced by TGF-β1 in transplant kidney interstitial fibrosis. *J. Cell. Mol. Med.* **21**, 2359–2369
31. Chandhoke, A. S., Karve, K., Dadakhujaev, S., Netherton, S., Deng, L., and Bonni, S. (2016) The ubiquitin ligase Smurf2 suppresses TGFβ-induced epithelial-mesenchymal transition in a sumoylation-regulated manner. *Cell Death Differ.* **23**, 876–888
32. Kavsak, P., Rasmussen, R. K., Causing, C. G., Bonni, S., Zhu, H., Thomsen, G. H., and Wrana, J. L. (2000) Smad7 binds to Smurf2 to form an E3 ubiquitin ligase that targets the TGF beta receptor for degradation. *Mol. Cell* **6**, 1365–1375
33. Lam, B. Q., Srivastava, R., Morvant, J., Shankar, S., and Srivastava, R. K. (2021) Association of diabetes mellitus and alcohol abuse with cancer: Molecular mechanisms and clinical significance. *Cells* **10**, 3077
34. Gross, J. L., de Azevedo, M. J., Silveiro, S. P., Canani, L. H., Caramori, M. L., and Zelmanovitz, T. (2005) Diabetic nephropathy: Diagnosis, prevention, and treatment. *Diabetes Care* **28**, 164–176
35. Tuleta, I., and Frangogiannis, N. G. (2021) Diabetic fibrosis. *Biochim. Biophys. Acta Mol. Basis Dis.* **1867**, 166044
36. Brosius, F. C., 3rd, Alpers, C. E., Bottinger, E. P., Breyer, M. D., Coffman, T. M., Gurley, S. B., Harris, R. C., Kakoki, M., Kretzler, M., Leiter, E. H., Levi, M., McIndoe, R. A., Sharma, K., Smithies, O., Susztak, K., *et al.* (2009) Mouse models of diabetic nephropathy. *J. Am. Soc. Nephrol.* **20**, 2503–2512
37. Azushima, K., Gurley, S. B., and Coffman, T. M. (2018) Modelling diabetic nephropathy in mice. *Nat. Rev. Nephrol.* **14**, 48–56
38. Khaddaj Mallat, R., Mathew John, C., Kendrick, D. J., and Braun, A. P. (2017) The vascular endothelium: A regulator of arterial tone and interface for the immune system. *Crit. Rev. Clin. Lab. Sci.* **54**, 458–470
39. Vigili de Kreutzenberg, S. (2021) Silent coronary artery disease in type 2 diabetes: A narrative review on epidemiology, risk factors, and clinical studies. *Explor. Med.* **2**, 1–19
40. Fu, J., Lee, K., Chuang, P. Y., Liu, Z., and He, J. C. (2015) Glomerular endothelial cell injury and cross talk in diabetic kidney disease. *Am. J. Physiol. Renal Physiol.* **308**, F287–297
41. Eleftheriadis, T., Pissas, G., Antoniadi, G., Liakopoulos, V., and Stefanidis, I. (2018) Allopurinol protects human glomerular endothelial cells from high glucose-induced reactive oxygen species generation, p53 overexpression and endothelial dysfunction. *Int. Urol. Nephrol.* **50**, 179–186
42. Tsai, Y. C., Kuo, M. C., Hung, W. W., Wu, L. Y., Wu, P. H., Chang, W. A., Kuo, P. L., and Hsu, Y. L. (2020) High glucose induces mesangial cell apoptosis through miR-15b-5p and promotes diabetic nephropathy by extracellular vesicle delivery. *Mol. Ther.* **28**, 963–974
43. Zeisberg, E. M., Tarnavski, O., Zeisberg, M., Dorfman, A. L., McMullen, J. R., Gustafsson, E., Chandraker, A., Yuan, X., Pu, W. T., Roberts, A. B., Neilson, E. G., Sayegh, M. H., Izumo, S., and Kalluri, R. (2007) Endothelial-to-mesenchymal transition contributes to cardiac fibrosis. *Nat. Med.* **13**, 952–961
44. Giordo, R., Ahmed, Y. M. A., Allam, H., Abusnana, S., Pappalardo, L., Nasrallah, G. K., Mangoni, A. A., and Pintus, G. (2021) EndMT regulation by small RNAs in diabetes-associated fibrotic conditions: Potential link with oxidative stress. *Front. Cell Dev. Biol.* **9**, 683594
45. Yu, C. H., Suriguga, Gong, M., Liu, W. J., Cui, N. X., Wang, Y., Du, X., and Yi, Z. C. (2017) High glucose induced endothelial to mesenchymal transition in human umbilical vein endothelial cell. *Exp. Mol. Pathol.* **102**, 377–383
46. Potenta, S., Zeisberg, E., and Kalluri, R. (2008) The role of endothelial-to-mesenchymal transition in cancer progression. *Br. J. Cancer* **99**, 1375–1379
47. Liu, X., Mujahid, H., Rong, B., Lu, Q. H., Zhang, W., Li, P., Li, N., Liang, E. S., Wang, Q., Tang, D. Q., Li, N. L., Ji, X. P., Chen, Y. G., Zhao, Y. X., and Zhang, M. X. (2018) Irisin inhibits high glucose-induced endothelial-to-mesenchymal transition and exerts a dose-dependent bidirectional effect on diabetic cardiomyopathy. *J. Cell. Mol. Med.* **22**, 808–822
48. Sabbineni, H., Verma, A., and Somanath, P. R. (2018) Isoform-specific effects of transforming growth factor β on endothelial-to-mesenchymal transition. *J. Cell. Physiol.* **233**, 8418–8428
49. Azhar, M., Runyan, R. B., Gard, C., Sanford, L. P., Miller, M. L., Andringa, A., Pawlowski, S., Rajan, S., and Doetschman, T. (2009) Ligand-specific function of transforming growth factor beta in epithelial-mesenchymal transition in heart development. *Dev. Dyn.* **238**, 431–442
50. Zeng, L., Wang, G., Ummarino, D., Margariti, A., Xu, Q., Xiao, Q., Wang, W., Zhang, Z., Yin, X., Mayr, M., Cockerill, G., Li, Y., Julie, Chien, S., Hu, Y., and Xu, Q. (2013) Histone deacetylase 3 unconventional splicing mediates endothelial-to-mesenchymal transition through transforming growth factor β2. *J. Biol. Chem.* **288**, 31853–31866
51. Derynck, R., Zhang, Y., and Feng, X. H. (1998) Smads: Transcriptional activators of TGF-beta responses. *Cell* **95**, 737–740
52. Massagué, J., and Chen, Y. G. (2000) Controlling TGF-beta signaling. *Genes Dev.* **14**, 627–644
53. Loeffler, I., Liebisch, M., Allert, S., Kunisch, E., Kinne, R. W., and Wolf, G. (2018) FSP1-specific SMAD2 knockout in renal tubular, endothelial, and interstitial cells reduces fibrosis and epithelial-to-mesenchymal transition in murine STZ-induced diabetic nephropathy. *Cell Tissue Res.* **372**, 115–133
54. Xu, B. H., Sheng, J., You, Y. K., Huang, X. R., Ma, R. C. W., Wang, Q., and Lan, H. Y. (2020) Deletion of Smad3 prevents renal fibrosis and inflammation in type 2 diabetic nephropathy. *Metab. Clin. Exp.* **103**, 154013
55. Yan, X., and Chen, Y. G. (2011) Smad7: Not only a regulator, but also a cross-talk mediator of TGF-β signalling. *Biochem. J.* **434**, 1–10
56. Nakao, A., Afrakhte, M., Morén, A., Nakayama, T., Christian, J. L., Heuchel, R., Itoh, S., Kawabata, M., Heldin, N. E., Heldin, C. H., and ten Dijke, P. (1997) Identification of Smad7, a TGFbeta-inducible antagonist of TGF-beta signalling. *Nature* **389**, 631–635

57. Rotin, D., and Kumar, S. (2009) Physiological functions of the HECT family of ubiquitin ligases. *Nat. Rev. Mol. Cell Biol.* **10**, 398–409
58. Zhang, Y., Chang, C., Gehling, D. J., Hemmati-Brivanlou, A., and Derynck, R. (2001) Regulation of Smad degradation and activity by Smurf2, an E3 ubiquitin ligase. *Proc. Natl. Acad. Sci. U. S. A.* **98**, 974–979
59. Lin, X., Liang, M., and Feng, X. H. (2000) Smurf2 is a ubiquitin E3 ligase mediating proteasome-dependent degradation of Smad2 in transforming growth factor-beta signaling. *J. Biol. Chem.* **275**, 36818–36822
60. Tang, L. Y., Yamashita, M., Coussens, N. P., Tang, Y., Wang, X., Li, C., Deng, C. X., Cheng, S. Y., and Zhang, Y. E. (2011) Ablation of Smurf2 reveals an inhibition in TGF-β signalling through multiple mono-ubiquitination of Smad3. *EMBO J.* **30**, 4777–4789
61. Bai, Y., and Ying, Y. (2020) The post-translational modifications of Smurf2 in TGF-β signaling. *Front. Mol. Biosci.* **7**, 128
62. Kushioka, J., Kaito, T., Okada, R., Ishiguro, H., Bal, Z., Kodama, J., Chijimatsu, R., Pye, M., Narimatsu, M., Wrana, J. L., Inoue, Y., Ninomiya, H., Yamamoto, S., Saitou, T., Yoshikawa, H., *et al.* (2020) A novel negative regulatory mechanism of Smurf2 in BMP/Smad signaling in bone. *Bone Res.* **8**, 41
63. Ohashi, N., Yamamoto, T., Uchida, C., Togawa, A., Fukasawa, H., Fujigaki, Y., Suzuki, S., Kitagawa, K., Hattori, T., Oda, T., Hayashi, H., Hishida, A., and Kitagawa, M. (2005) Transcriptional induction of Smurf2 ubiquitin ligase by TGF-beta. *FEBS Lett.* **579**, 2557–2563
64. Yan, X., Liu, Z., and Chen, Y. (2009) Regulation of TGF-beta signaling by Smad7. *Acta Biochim. Biophys. Sin.* **41**, 263–272
65. Ogunjimi, A. A., Briant, D. J., Pece-Barbara, N., Roy, C. L., Guglielmo, G. M. D., Kavsak, P., Rasmussen, R. K., Seet, B. T., Sicheri, F., and Wrana, J. L. (2005) Regulation of Smurf2 ubiquitin ligase activity by anchoring the E2 to the HECT domain. *Mol. Cell* **19**, 297–308
66. Medici, D., Potenta, S., and Kalluri, R. (2011) Transforming growth factor-β2 promotes Snail-mediated endothelial-mesenchymal transition through convergence of Smad-dependent and Smad-independent signalling. *Biochem. J.* **437**, 515–520
67. Ursoli Ferreira, F., Eduardo Botelho Souza, L., Hassibe Thomé, C., Tomazini Pinto, M., Origassa, M., Salustiano, S., Marcel Faça, V., Olsen Câmara, N., Kashima, S., and Tadeu Covas, D. (2019) Endothelial cells tissue-specific origins affects their Responsiveness to TGF-β2 during endothelial-to-mesenchymal transition. *Int. J. Mol. Sci.* **20**, 458
68. Ramachandran, A., Vizán, P., Das, D., Chakravarty, P., Vogt, J., Rogers, K. W., Müller, P., Hinck, A. P., Sapkota, G. P., and Hill, C. S. (2018) TGF-β uses a novel mode of receptor activation to phosphorylate SMAD1/5 and induce epithelial-to-mesenchymal transition. *eLife* **7**, e31756
69. Sniegon, I., Prieß, M., Heger, J., Schulz, R., and Euler, G. (2017) Endothelial mesenchymal transition in hypoxic microvascular endothelial cells and paracrine induction of cardiomyocyte apoptosis are mediated via TGFβ$_1$/SMAD signaling. *Int. J. Mol. Sci.* **18**, 2290